

## 2 Wind-Waves and Atmospheric Shear Stress

---

Wind and wave relations for the shallow waters of Laguna Madre were investigated for the purpose of evaluating modeling approaches for wind-wave shear stresses. Wave and current data from shallow, open-water areas in Laguna Madre were analyzed as a first step in a study of shear stresses. Measured pressures and velocity components were used to estimate significant wave height, spectral-peak wave period, depth, mean current speed, and wave orbital flow components at 30-minute intervals. Using previous scalings, dimensionless wave energy and depth were found to be related differently in water depths less than 2 m (including areas with submersed aquatic vegetation) than in deeper, bare areas in this and previous studies. Waves in ultra-shallow water were more consistently depth limited, and dimensionless energies and periods were less than expected for the same dimensionless depth. Furthermore, wave characteristics scaled by wind speed were not consistent among stations of different depths.

A rescaling of wave energy and period by atmospheric friction velocity was performed. Direct measurements of atmospheric shear stress were not made as part of this study, but previous relationships for the atmospheric roughness height and friction factor  $C_d$  were evaluated according to the wind and wave data. Dimensionless wave parameters were better related, and resulting wave hindcasts had smaller errors, using the new wave scaling by atmospheric friction velocity. Rescaled dimensionless energies and periods allowed the development of new expressions for wave height and period that were based on water depth and  $C_d$ .

A new expression for  $C_d$  in terms of water depth and wind speed is proposed. In vegetated areas, an effective water depth from the water surface to the seagrass canopy height was used. The fraction of atmospheric shear stress going into waves, as opposed to that going into currents, was found to decrease as the inverse of the square-root of wind speed for wind speeds greater than 5 m/sec.

### Background

#### Atmospheric shear stress

Atmospheric shear stress ( $\tau_a$ , Pa) was calculated on the basis of wind speed  $U_a$ , in meters per second, at 10-m height:

$$\tau_a = \rho_a C_d U_a^2 \quad (1)$$

where  $\rho_a$  is the air density (about 1.225 kg/m<sup>3</sup>), and  $C_d$  is the atmospheric friction factor appropriate for wind referenced to 10-m height (CERC 1984). An important component of atmospheric shear stress comes from wave roughness at various scales, and  $C_d$  generally increases with increased wind speed, at least up to some high wind speed. The main transfer of momentum from the atmosphere to waves occurs at relatively short wave lengths of about 0.3-m (range 0.06 to 1 m) wavelength (Gemrich et al. 1994) but transfer to slightly longer wavelengths is also appreciable (Donelan 1990; and Lionello et al. 1998). Short waves are advected by the long-wave orbitals, reducing wind speed relative to short waves at long-wave crests and diminishing the importance of short-wave roughness to atmospheric drag. The wind field is modified by dominant wavelengths (Lionello et al. 1998). Significant wave height  $H_s$  is the most often used, physically important, length scale used to estimate  $C_d$ . When waves are fetch- and/or duration-limited, however, the stage of wave development affects  $C_d$ . For a constant wind speed,  $C_d$  decreases as waves become higher, longer, and less steep.

With an assumed logarithmic velocity profile and neutral atmospheric stability, the atmospheric friction factor is dependent on surface roughness

$$C_d = \left( \frac{\kappa}{\ln(10/z_o)} \right)^2 \quad (2)$$

where  $\kappa$  is the von Karman constant (0.4), and  $z_o$  is the surface roughness coefficient in meters. The latter is much smaller than  $H_s$ . At wind speeds greater than about 2.5 m/sec, those important in this study, air flow becomes aerodynamically rough and  $z_o$  is approximately a quadratic function of wind speed (Donelan 1990). For the turbulent-rough regime, Hsu (1974) related  $z_o$  to both wave steepness (significant wave height  $H_s$  over wave length  $L_w$ ) and wave age (wave celerity  $C$  over atmospheric friction velocity  $U_{*a}$ ) starting with

$$z_o = \frac{H_s}{g L_w} U_{*a}^2 \quad (3)$$

and then substituting a deep-water relationship for  $L_w$  to obtain

$$z_o = \frac{H_s}{2 \pi C^2} U_{*a}^2 \quad (4)$$

Hsu originally compared this latter formulation to a number of data sets, and recent comparisons have also found it to be reliable (Donelan 1990).

Various expressions have been developed for  $C_d$ . For fully-developed oceanic wave conditions, Hsu (1988) developed the following expression for  $C_d$  from Equation 2 by setting the ratio of  $C$  to  $U_{*a}$  equal to 29 and substituting an analytical expression for  $H_s$  into Equation 4:

$$C_d = \left( \frac{0.4}{14.56 - 2 \ln U_a} \right)^2 \quad (5)$$

Various linear expressions have been proposed that relate  $C_d$  to  $U_a$ . For example, for oceanic conditions and neutral atmospheric stability, Wu (1980) proposed  $C_d = (8.0 + 0.65 U_a) \times 10^{-4}$ , while Atakturk and Katsaros (1999) found  $C_d = (8.7 + 0.78 U_a) \times 10^{-4}$  for Lake Washington, Washington.

The roughness height has also been related to Charnock's parameter  $\alpha_c$  to include the effect of wave development

$$z_o = \alpha_c U_{*a}^2 / g \quad (6)$$

Reported field values for  $\alpha_c$  generally range from 0.012 to 0.035 for "old" and "young" waves respectively (Wu 1980; Hsu 1988; and Lionello et al. 1998). During the initial stage of wave development, roughness heights are much greater. Wu recommended using  $\alpha_c = 0.0185$  in Equation 6 and proposed an additional term based on dimensional arguments

$$z_o = \frac{\alpha_c U_{*a}^2}{g} \left( \frac{\mu U_{*a}}{\gamma} \right)^{\beta-2} \quad (7)$$

where  $\mu$  is the dynamic viscosity of water, and  $\gamma$  is the surface tension. Wu suggests that the value of the exponent  $2 < \beta < 2.5$  correctly defines the dependence of  $z_o$  on  $U_{*a}$ .

Janssen (1989) developed the following relationship for wave roughness:

$$z_o = \frac{\alpha_{cr} U_{*a}^2}{g(1 - \tau_{aw}/\tau_a)^{1/2}} \quad (8)$$

where  $\tau_{aw}$  is the atmospheric shear-stress going into the waves, and  $\alpha_{cr}$  is a reference or reduced Charnock's parameter ( $\approx 0.01$ ). Lionello et al. (1998) used Equation 8 to test two-way coupling for atmospheric and ocean-wave models.

### Shear stress budget

Reported values for the fraction of momentum transferred from the atmosphere to waves vary widely. Lionello et al. (1998) indicate that  $\tau_a > \tau_{aw} > 0.15\tau_a$ . As with surface roughness, the stage of wave development affects the fraction of momentum transferred from the atmosphere to waves. "Young," steep waves absorb a greater fraction of atmospheric shear stress as waves develop. Equations 6 and 8 suggest that

$$\frac{\tau_{aw}}{\tau_a} = 1 - (\alpha_{cr}/\alpha_c)^2 \quad (9)$$

which implies that the shear-stress fraction transferred to waves is related to wave age, with about 95 percent of  $\tau_a$  transferred to  $\tau_{aw}$  during initial wave development and about 40 percent for old waves. Apparently, wave dissipation mechanisms more effectively shunt momentum into currents for old waves.

In a fully-developed wave field, when temporal and spatial variations of wave spectra are minimal, shear-stress input from the atmosphere is about equal to wave dissipation. Wave dissipation comes from various losses: friction, wave-wave interactions, white capping, and wave breaking. Wave breaking occurs in deep water when the wave steepness reaches or exceeds 0.14, and in shoaling water when the wave height exceeds about 80 percent of the depth (CERC 1984). White-capping occurs when wind separates at and de-stabilizes wave crests and especially when  $C/U_{*a} < 1$  (Wu 1980). The resulting loss of wave energy is converted into mean-flow momentum and to turbulent mixing. Wave dissipation is not well understood in general, but it is recognized as important to momentum transfer from the atmosphere to the water column (Lionello et al. 1998). No consensus exists among researchers about the relative magnitudes of dissipation mechanisms, and more research is probably needed before a consensus can be reached.

For open-ocean, deep-water conditions, most of the atmospheric input eventually goes to the upper part of the water column (Richman and Garrett 1977). In shallow-water, however, wave shear-stresses transmitted to the bed can be of the same order as the atmospheric shear stresses. For example, Sanford (1994) measured wave conditions during a January-1990 wind-wave resuspension event at a 3.4-m deep tripod station near Pooles Island in Upper Chesapeake Bay and estimated the wave shear stress to be 0.6 Pa at the bed. Winds were offshore at 11 m/sec and  $\tau_a$  was apparently about 0.25 Pa. If in fact wave shear stress is of the same order as  $\tau_a$ , less of the total  $\tau_a$  input is transferred to currents in shallow water than in deeper water.

### Depth-limited waves for unvegetated bottoms

Analytical models for waves in shallow water are based on dimensionless parameters used to collapse data to power-law relations. For depth-limited, but otherwise fully-developed, waves, models are of the form

$$E^* = a_1 h^{*a_2} \quad (10)$$

$$f^* = a_3 h^{*a_4} \quad (11)$$

where  $E^* = g^2 E / U_a^4$  is dimensionless wave energy,  $h^* = gh / U_a^2$  is dimensionless depth,  $f^* = U_a / g T_p$  is dimensionless wave frequency,  $E = \sigma^2$  is the variance of the wave height field, and  $E = H_s^2 / 16$ ,  $U_a$  is the wind speed adjusted to 10 m height in meters per second, and  $T_p$  is the spectral-peak wave period in seconds. CERC (1984) found the coefficients to be  $a_1 = 1.4 \times 10^{-3}$ ,  $a_2 = 1.5$ ,  $a_3 = 0.16$ , and  $a_4 = -0.375$ . Young and Verhagen (1996) found coefficients for Equations 10 and 11 to be  $a_1 = 1.06 \times 10^{-3}$ ,  $a_2 = 1.3$ ,  $a_3 = 0.20$ , and  $a_4 = -0.375$ .

Formulations that include the effects of fetch length are slightly more complicated. The depth-limited and deep-water cases form asymptotic limits which include the dimensionless fetch length  $X^* = gx / U_a^2$  where  $x$  is the fetch length. For example, Young and Verhagen (1996) found

$$E^* = 3.64 \times 10^{-3} \left( \underset{\text{where}}{\tanh A_1 \tanh \left[ \frac{B_1}{\tanh A_1} \right]} \right)^{1.74} \quad (12)$$

$$A_1 = 0.493 h^{*0.75}, \quad B_1 = 3.13 \times 10^{-3} X^{*0.57} \quad (13)$$

### Wave friction formulations

The wave shear stress at the bed  $\tau_{wb}$  is calculated as follows:

$$\tau_{wb} = \frac{1}{2} f_w \rho U_{wbm}^2 \quad (14)$$

Some friction formulation must be assumed for  $f_w$ . For example, Luettich et al. (1990), Bailey and Hamilton (1997), Hamilton and Mitchell (1996), and Hawley and Lesht (1992) used the laminar wave friction formulation where

$$f_w = 2 \left( \frac{U_{wbm} A_{bm}}{\nu} \right)^{-0.5}, \quad \frac{U_{wbm} A_{bm}}{\nu} \leq 10^4 \quad (15)$$

and  $\tau_{wb}$  is the instantaneous maximum wave shear stress at the bed,  $f_w$  is the wave friction factor,  $U_{wbm}$  is the maximum wave orbital speed just above the bed,

$$U_{wbm} = \frac{\pi H_s}{T_p \sinh(2\pi h/L_w)} \quad (16)$$

$A_{bm}$  is the maximum wave excursion amplitude at the bed,

$$A_{bm} = 2\pi U_{wbm}/T_p \quad (17)$$

and  $\nu$  is the kinematic viscosity of water. The term in parentheses on the right side of Equation 15 is the wave Reynolds number just above the bed. For unvegetated beds,  $U_{wbm}$  and  $A_{bm}$  are computed at the bed and become appreciable when the wave length is about twice the water depth. In seagrass beds, however, the wave begins to "feel" friction when the wave length is twice the distance from the water surface to the top of the plant canopy since the canopy-top presents appreciable friction to flow. With respect to waves, seagrass beds are shallower (by about the height of the canopy) than the water-column depth.

Laminar wave-friction factors are greater than turbulent, smooth, or rough friction factors used in other situations (Kamphuis 1975). Even though wave Reynolds numbers for waves may be low enough to meet viscous-dominated criteria (about  $10^4$ ) developed in laboratories, field conditions most often include a turbulent water column and finite currents. Langmuir circulation cells having appreciable vertical circulations are common in the lagoon. Turbulence intensities are higher than normal in seagrass beds due to the shedding of vortices by plant components, and a turbulent criterion has not been developed for these flows.

Kamphuis (1975) developed a turbulent-rough formulation

$$f_w = 0.4 \left( \frac{k_n}{A_{bm}} \right)^{0.75}, \quad \frac{A_{bm}}{k_n} < 50 \quad (18)$$

where  $k_n$  is a roughness height normally about twice the bed-grain diameter at the 90<sup>th</sup> percentile for plane beds. A similar rough formulation was used by Christoffersen and Jonsson (1985) in their model of combined wave and current friction.

## Measurements and Data Processing

### Waves and currents

Measurements of waves and currents were specifically carried out for this study. Pressure and velocity data were collected by Conrad Blucher Institute (CBI) and transmitted to WES as part of the interagency study of possible dredged- material dispersal impacts. Pressures were measured with Keller Semi-Conductor ® model PA10 strain gauges. Velocities were measured with Marsh-McBirney ® electromagnetic current meters. Data were logged on Applied Microsystems ® Smart Packs.

Measurements were taken at six sites located in Upper (U) and Lower (L) Laguna Madre. Approximate locations for stations are shown in Figure 2 with the exception of station U1w, which is actually located in southern Corpus Christi Bay. The fetch lengths to the 0.5-m depth contour for the dominant wind direction were determined for select locations and are presented in Table 3.

Station	Julian Days of Data	Latitude N	Longitude W	Fetch Length to 130°, km
L1w	14-50	26° 10.7500'	97° 15.6000'	10.2
L2w	14-33	26° 08.0833'	97° 12.4666'	5.1
L3w	15-49	26° 35.4200'	97° 22.9600'	4.6
U1w	10-43	27° 41.4580'	97° 13.2960'	3
U2w	23-32	27° 17.2333'	97° 24.7500'	3.7
U3w	14-38	27° 11.5500'	97° 25.7000'	3

Julian days refer to the days of the year in 1998. Station L1w was located on an azimuth of 310° from L2w, down-wind along the dominant wind direction (130°). Station L2w was located in a *Thalassia testudinum* seagrass area. Station L1w had a bare bottom, and stations L3w and U3w were near the edges of *Syringodium filiforme* and *Halodule wrightii* seagrass beds.

Gauges recorded 5-Hz bursts of data every 30 min. Data were in blocks of about 6 min, each block containing about 3,000 readings of pressure, and  $u$ - and  $v$ -velocity components.

Sub-surface measurements were used to estimate significant wave height, spectral-peak wave period, depth, mean-current speed, and wave-orbital flow components at 30-min

intervals. The mean pressure was converted to the water depth over the gauge. Pressure fluctuations were adjusted from the measurement depth to the water surface by a calculation that involved wave length, total depth and depth of submergence of the gauge (Dean and Dalrymple 1991). Significant wave height  $H_s$  was calculated as

$$H_s = 4\sigma \quad (19)$$

where  $\sigma$  is the standard deviation of the adjusted pressure (db) measurements.

Spectra of pressure and velocity components were computed with Splus® statistical software for each sampling burst. Six-minute bursts of about 3,000 points were detrended, demeaned, tapered (10 percent cosine), and converted to spectral density in the frequency domain. Spectra were smoothed to reduce variability, and the spectra peaks that occurred between 0.5- to 8-sec periods were identified. The magnitudes of the velocity component peaks were determined by first fitting a regression line through the spectral region outside the peak band from 0.66 to 1.5 of the peak frequency. The magnitude was then determined as the difference between the regression line and the spectral line at the wave peak frequency. Example smoothed spectra for pressure,  $u$ - and  $v$ - velocity components, and an example velocity-component spectrum and locally-weighted regression line are shown in Figure 5.

Wave characteristics estimated from bursts were smoothed with a 3-hr low-pass filter and decimated to 1-hr intervals. A comparison of the distributions for raw- and smoothed-wave heights for L1w is shown in Figure 6.

Wave length estimation was based on iteration of the dispersion equation:

$$L_w = \frac{gT_p^2}{2\pi} \tanh(2\pi h/L_w) \quad (20)$$

where an iteration convergence criteria of  $2 \times 10^{-5}$  m was used, and wave celerity was calculated as  $C = L_w/T_p$ .

As an indication of the quality and/or consistency of the wave and current data, the root-sum-squares of the maximum wave-induced current components were plotted against the calculated peak currents. Linear wave theory was applied to calculate peak currents from the wave data. Results are shown in Figure 7 for L1w. The residual standard error is 1.4 cm/sec and the  $R^2 = 0.95$  for this comparison. One source of discrepancy at low values might have come from a zero-flow offset in the electro-magnetic current meter data. Such an offset would be consistent with a comparison made to previous Doppler current meter data taken at the same site to be described later.

## Wind conditions

Wind data from South Padre Island, Rincon, and Bird Island stations maintained by CBI were downloaded from their web site (<<http://tcoon.cbi.tamcc.edu/data>>) and used in the analysis of wave data. These stations span most of the length of Laguna Madre, as shown in Figure 2, but were many miles from the wave gauges. For this period,  $u$ - and  $v$ - component

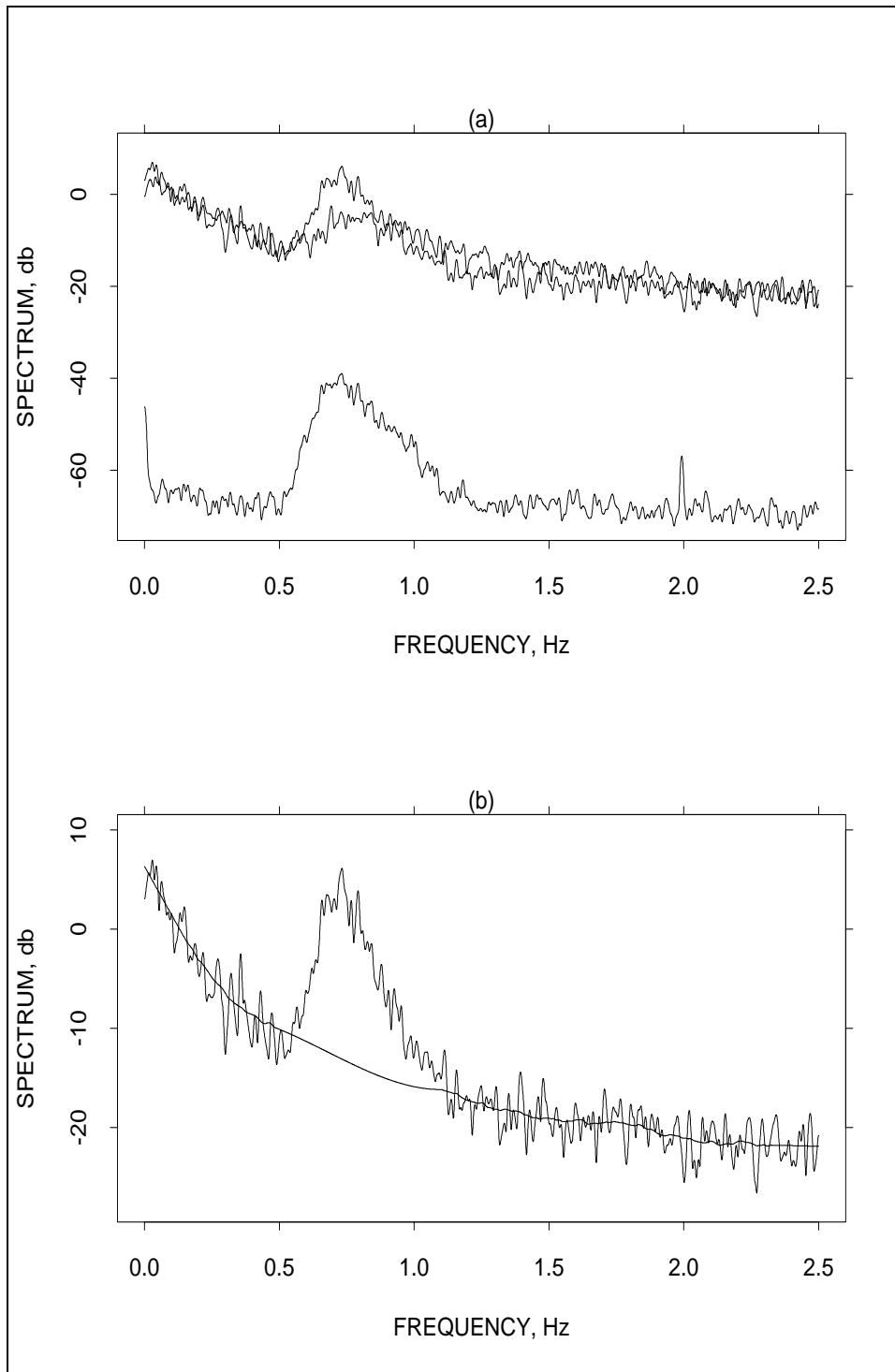


Figure 5. Example measurement spectra (a) for current component and pressure signals, and (b) with regression line fit to velocity component to determine peak height

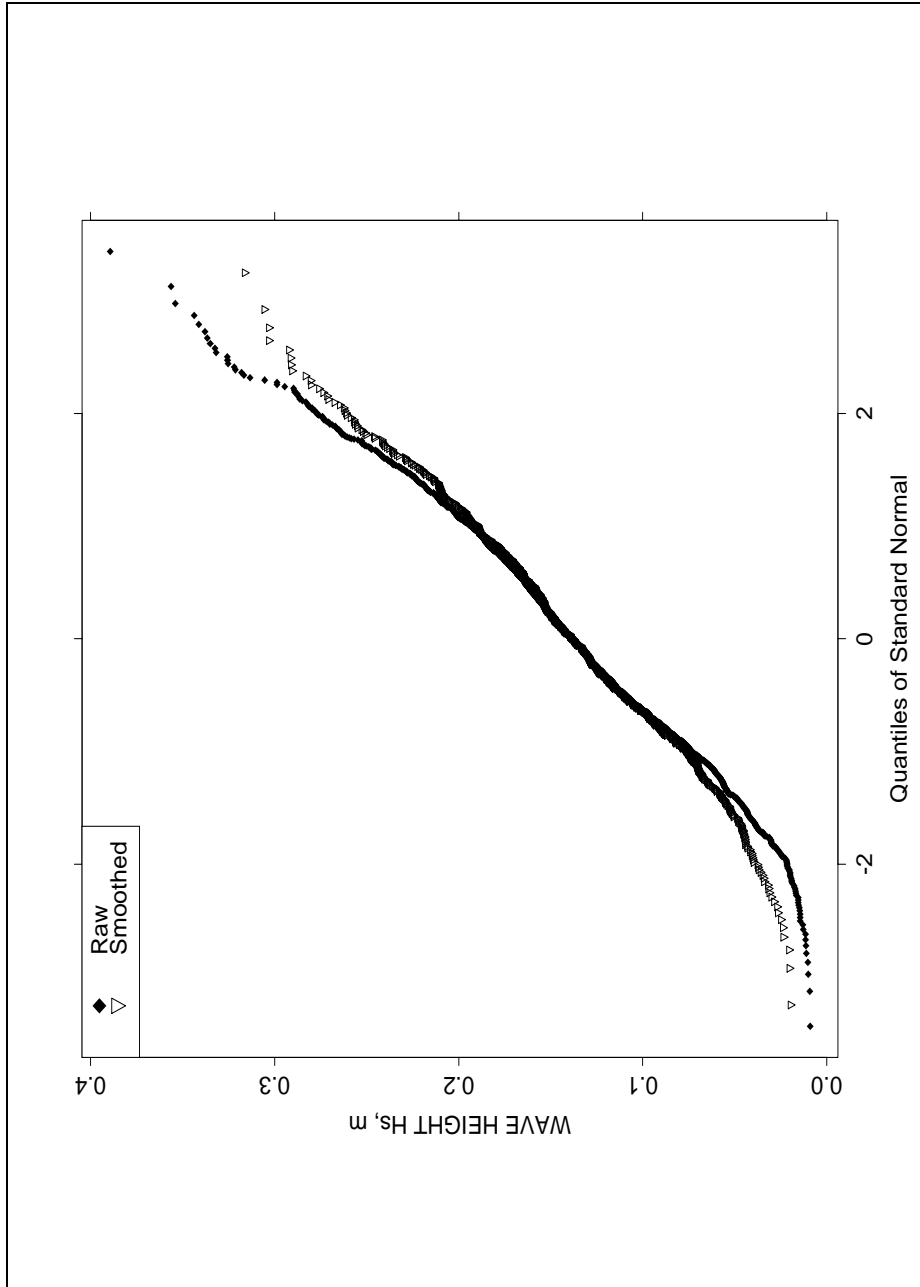


Figure 6. The statistical distributions of raw and 3-hr low-pass smoothed wave heights

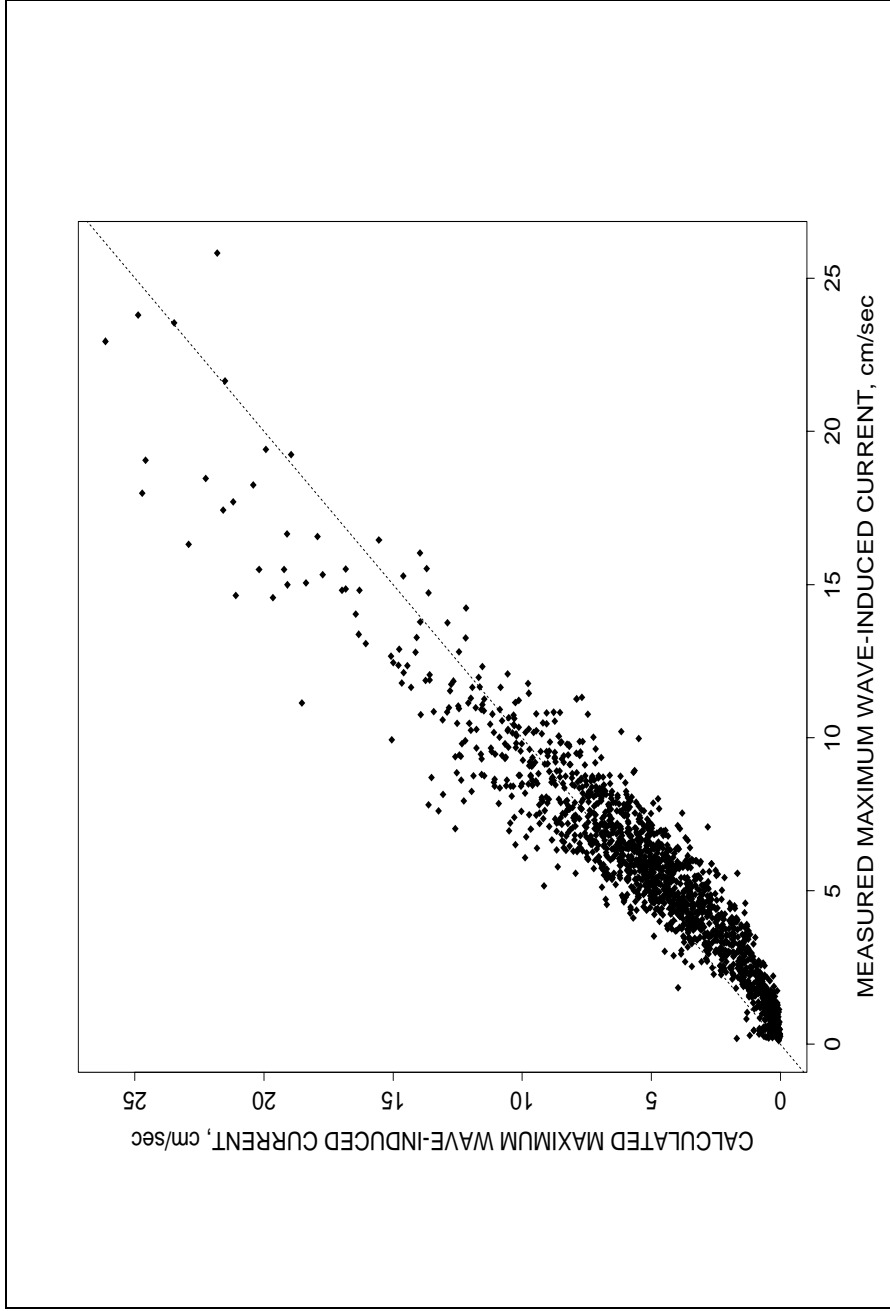


Figure 7. Comparison of measured maximum near-bed wave currents with those calculated from wave characteristics and linear wave theory

wind data from the three stations were combined, and a locally-weighted regression was used to perform 3-hour low-pass filtering of the data. To make the comparison of wind and wave data meaningful, wind data were scrutinized to ensure that they were representative of the wave measurement sites. In addition to averaging and filtering, time periods were identified when wind conditions were (a) relatively uniform over the area (identified by plotting and comparing the winds from the three stations) and (b) from the dominant southeasterly direction (identified by averaging wind direction from the three stations and taking wind directions from 110 to 145°). The concern was that data taken during frontal passage events, or when the wind record might be corrupted by some other factor, should not be used. Statistical distributions of raw and 3-hr low-pass filtered wind speeds are shown in Figure 8 for Julian day 13 through 33. A histogram of wind directions for this period is shown in Figure 9.

### Observational results

A period from about 1998 Julian day 13 through 50 was found to have the longest continuous data coverage, and all available data were compiled for this period.

**Wave conditions.** Table 4 summarizes wave characteristics, wave steepness ( $H_s/L_w$ ), and relative depth ( $h/L_w$ ). Histograms of  $H_s$  and  $T_p$  are shown in Figures 10 and 11 for the six stations. For plotting purposes, wave heights and periods for U1w were cut off at 0.5 m and 3.8 sec, even though a very small number of data reached 0.65 m and 6.7 sec.

**Current conditions.** Current speed  $U$  values were relatively low (median values of 7 cm/sec or less). Current conditions are summarized for  $U$  and for the N-S and E-W components ( $u$  and  $v$ ) in Table 5. Current magnitude  $U$  statistics were compiled from smoothed-current data, while  $u$ - and  $v$ -component statistics are based on raw data.

Current data were previously collected near L1w in 1994-1995 by CBI, using an acoustic-Doppler velocimeter (Brown and Kraus 1997). The present measurement results indicate a residual flow to the ESE at L1w that was not shown in the previous CBI current data. The axis of the scattered data has a similar direction but is offset to the ESE by perhaps 5 cm/sec.

## Results and Discussion

### Atmospheric friction factors

The expressions of Hsu (1974) for atmospheric roughness height,  $z_o$ , presented in Equations 3 and 4 are not equivalent for shallow water when  $h/L_w$  values are less than 0.5 and, therefore,  $\tanh(2\pi h/L_w)$  values are less than 1.0 as in deep water. Based on Hsu's development, it might be assumed that Equation 3 is more suitable for shallow water than Equation 4 if wave steepness is the primary parameter affecting  $z_o$ .

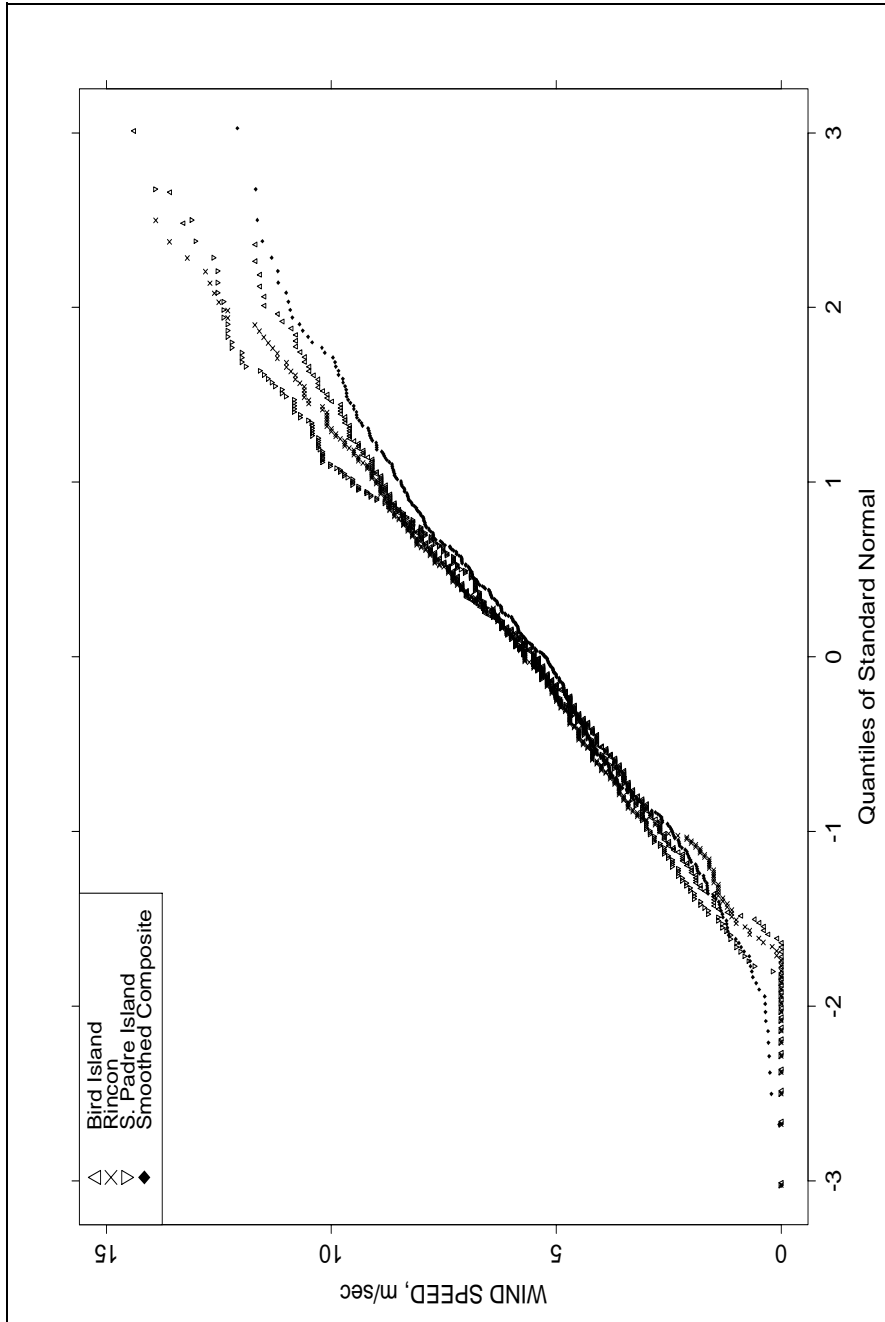


Figure 8. The statistical distributions of raw wind speeds from three stations and 3-hr low-pass smoothed wind speed

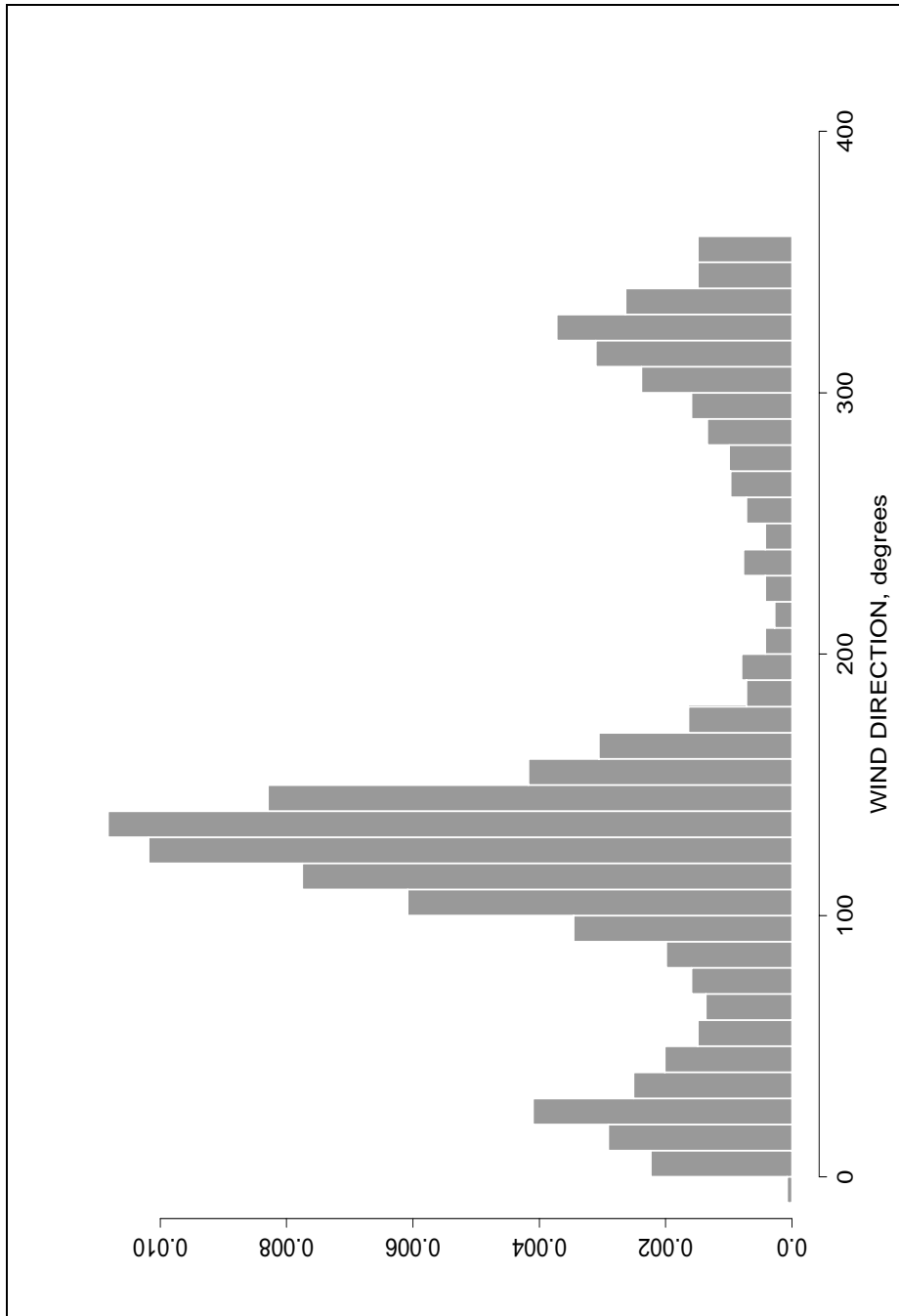


Figure 9. Histogram of wind direction for the study period

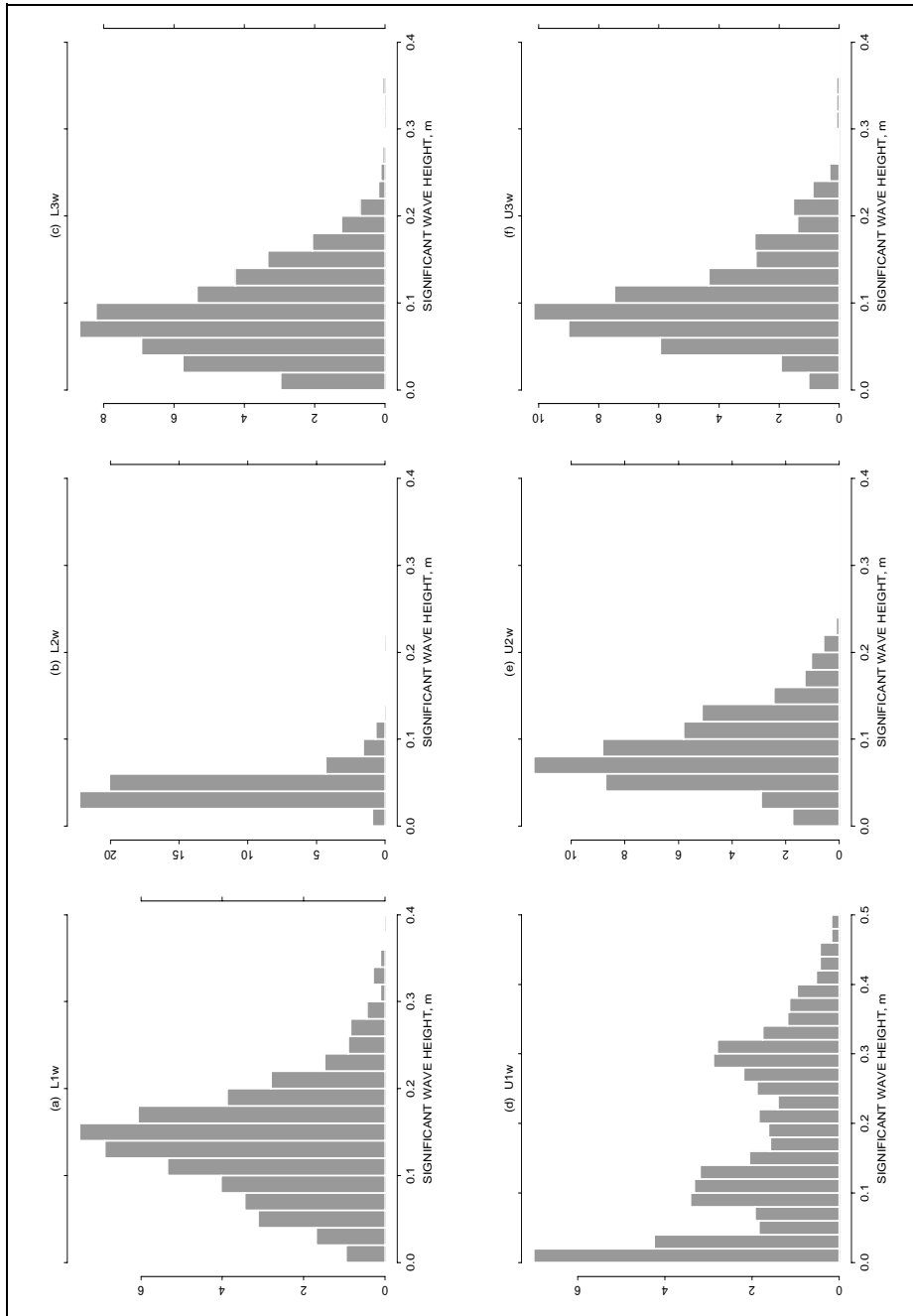


Figure 10. Histograms of significant wave heights for the six measurement stations

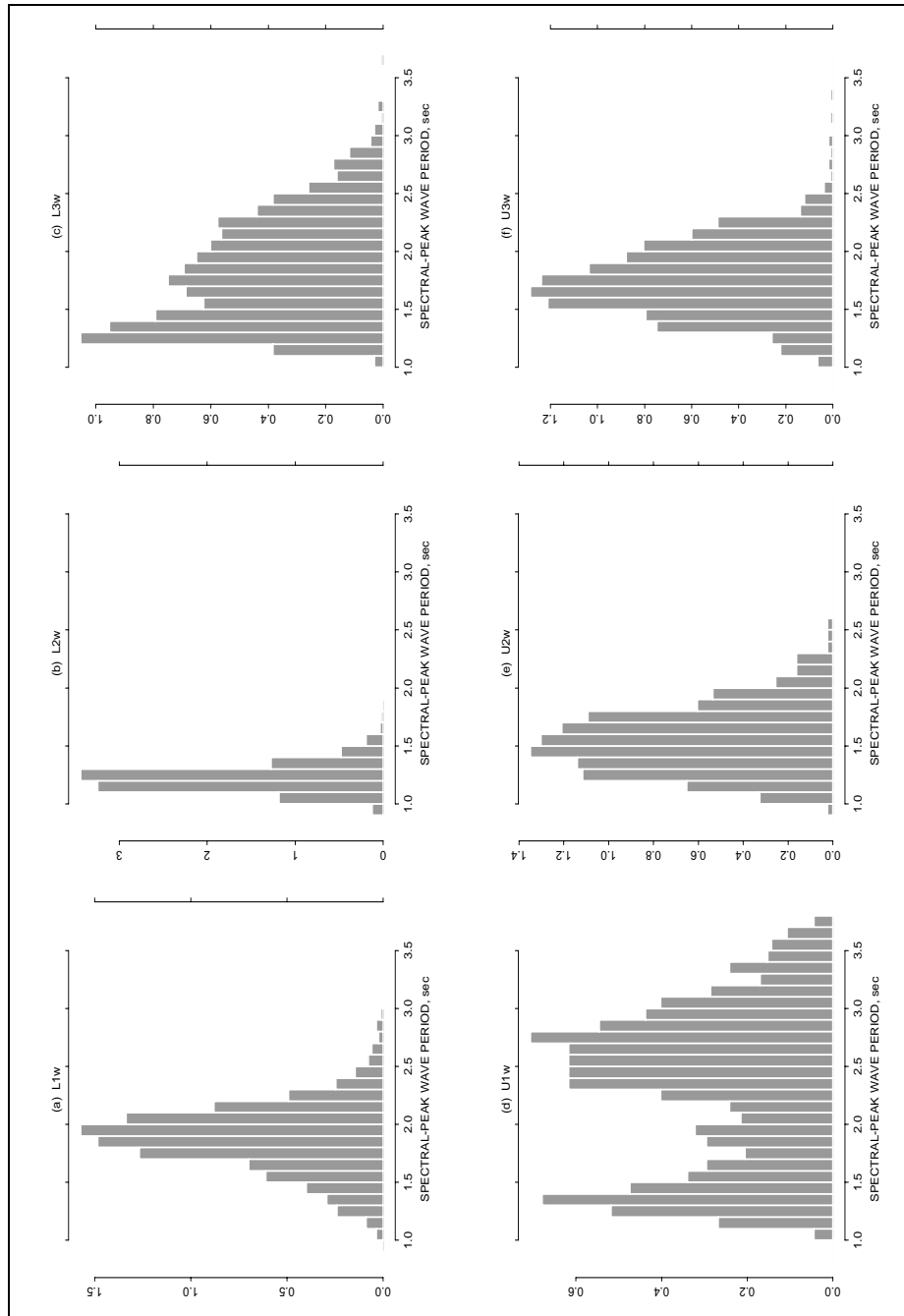


Figure 11. Histograms of peak wave periods for the six measurement stations

Table 4 Summary of Wave Gauge Observations						
Station	L1w	L2w	L3w	U1w	U2w	U3w
$h$ (m) Mean (Std. Dev.)	2.07 (0.10)	1.13 (0.10)	1.79 (0.06)	2.39 (0.11)	1.57 (0.06)	1.61 (0.12)
$H_s$ (m) Mean (Std. Dev.)	0.14 (0.055)	0.04 (0.017)	0.09 (0.033)	0.16 (0.109)	0.09 (0.035)	0.10 (0.046)
Percentiles: 25	0.10	0.03	0.06	0.07	0.06	0.07
50	0.14	0.04	0.08	0.13	0.08	0.09
75	0.17	0.05	0.11	0.25	0.11	0.12
$T_p$ (sec) Mean (Std. Dev.)	1.87 (0.250)	1.22 (0.107)	1.81 (0.357)	2.33 (0.508)	1.54 (0.239)	1.75 (0.250)
Percentiles: 25	1.72	1.14	1.53	1.93	1.39	1.56
50	1.89	1.20	1.76	2.33	1.53	1.73
75	2.03	1.27	2.07	2.68	1.70	1.92
$H_s/L_w \times 100$ Mean (Std. Dev.)	2.46 (0.6)	1.85 (0.4)	1.87 (0.9)	2.03 (1.1)	2.37 (0.3)	2.10 (0.5)
Percentiles: 25	2.11	1.53	1.25	1.05	1.89	1.79
50	2.51	1.78	1.69	2.23	2.46	2.08
75	2.89	2.15	2.34	2.85	2.85	2.46
$h/L_w$ Mean (Std. Dev.)	0.41 (0.119)	0.50 (0.064)	0.40 (0.137)	0.34 (0.141)	0.46 (0.153)	0.36 (0.088)
Percentiles: 25	0.33	0.45	0.28	0.24	0.35	0.30
50	0.38	0.50	0.38	0.29	0.43	0.35
75	0.45	0.54	0.49	0.41	0.53	0.43

Table 5 Summary of Current Observations						
Station	L1w	L2w	L3w	U1w	U2w	U3w
<i>U</i> (cm/sec) Mean (Std. Dev.)	7.02 (2.44)	4.55 (2.97)	2.19 (1.17)	6.88 (3.68)	4.60 (1.01)	5.07 (1.91)
Percentiles: 25	5.30	2.19	1.41	4.54	3.30	3.40
50	6.55	3.58	1.91	5.78	4.09	4.82
75	8.35	6.61	2.66	8.72	5.57	6.22
<i>u</i> (cm/sec) Mean (Std. Dev.)	-2.23 (4.04)	-2.30 (3.51)	0.18 (1.59)	-2.89 (6.89)	-0.55 (2.24)	0.25 (4.20)
Percentiles: 25	-4.81	-5.08	-0.77	-7.13	-1.85	-2.33
50	-2.44	-1.60	0.15	-2.63	-0.54	0.15
75	0.31	0.50	1.17	2.13	0.90	2.35
<i>v</i> (cm/sec) Mean (Std. Dev.)	3.74 (4.89)	2.89 (2.32)	0.08 (2.14)	-0.26 (4.62)	0.47 (1.31)	3.20 (1.63)
Percentiles: 25	0.64	1.03	-1.37	-2.78	-0.23	2.40
50	3.96	2.50	-0.04	-0.55	0.53	3.15
75	7.09	4.68	1.26	2.53	1.31	4.09

Equations 3 and 4 were tested in a comparison to previous observed values and by correlation to wind speed. These equations were substituted into Equation 2, and wind and wave data were used to calculate atmospheric friction factors  $C_d$ . Iteration was required since  $U_{*a}$  depends on  $C_d$ . New  $U_{*a}$  values were computed and  $C_d$  re-estimated until the maximum change in  $C_d$  over the time series was less than  $2 \times 10^{-6}$  per iteration. Those  $C_d$  values calculated with Equation 4 were consistently better correlated to  $U_a$  and had much less scatter than those calculated with Equation 3, despite the fact that  $h/L_w$  values for the various stations ranged from 0.24 to 0.45 at the 25<sup>th</sup>-percentile longest waves.

Atmospheric friction factor  $C_d$  values calculated with Equation 4 were cast into a linear form versus wind speed such that

$$C_d = (6.49 + C_{cd}U_a) \times 10^{-4}, \quad U_a > 2 \text{ m/sec} \quad (21)$$

where the six stations had a common intercept.  $C_{cd}$  data were separated into directional bands corresponding to the directional modes seen in Figure 9, and regressions were performed on each of three bands. Results for the six stations are presented in Table 6.

Table 6 Coefficients for Equation 21 for Wind Direction Bands				
$C_{cd} \times 10$				
Station	Wind Direction			
	All	< 80°	80° to 250°	> 250°
L1w	9.61	9.47	9.1	9.96
L2w	7.71	8.61	7.27	8.4
L3w	7.58	8.04	8.55	7.61
U1w	9.24	9.91	8.76	9.28
U2w	8.12	9.03	8.24	7.31
U3w	8.77	8.8	8.42	9.03

Station L2w located in a seagrass bed had relatively small waves and lower friction factors (13 percent lower at 10 m/sec wind speed) than L1w. It should be noted that station U1w is located in Corpus Christi Bay, and data obtained here were processed only for comparison. Some stations displayed wind-direction dependence with respect to  $C_{cd}$ . It appears that the directional  $C_{cd}$  values do not correlate well to the corresponding fetches. Differences in  $C_{cd}$  appear to be caused by depth and bed condition or seagrass type, as will be discussed below.

The finding that Equation 4 is better correlated to wind speed than is Equation 3 suggests that wave age is more strongly related to  $z_o$  than is wave steepness  $H_s/L_w$ . Wu (1980) also argued that wave steepness based on the dominant waves is not a sound physical scaling for

atmospheric roughness. Furthermore, Equation 4 suggests there might be a relationship between two dimensionless parameters such that

$$\frac{z_o}{H_s} \propto \left( \frac{C}{U_{*a}} \right)^n \quad (22)$$

which is similar to a relationship that Donelan (1990) used. Both these dimensionless parameters are strongly related to the wind speed. Equation 22 with  $n = -2$  is equivalent to Equation 4 and regression results indicated a multiple correlation squared ( $M-R^2$ ) = 0.978 and residual standard error (RSE) = 0.0686 for  $n = 2056$ . However, it was found through successive approximation of  $z_o$  and  $U_{*a}$  that  $n = -1.57$  gave the best fit for Equation 22 ( $M-R^2 = 0.984$ , RSE = 0.0468,  $n = 2056$ ). Thus, a new empirical relationship for the atmospheric roughness height was obtained:

$$z_o = 0.0493 H_s \left( \frac{U_{*a}}{C} \right)^{1.57} \quad (23)$$

Equation 23 was more consistent with the present data with respect to the residual standard error. However, the exponent of Equation 23 is much lower than those compiled by Donelan, whose exponents ranged from about 2 to 4. The addition of the dimensionless term introduced in Equation 7 to the right side of Equation 22 did not improve the fit or suggest a different value for the exponent.

Values of  $C_d$  computed with Equations 4 and 23 increased more quickly with wind speed than did the linear relationships previously presented, as shown in Figure 12 for L1w. In shallow water,  $C$  is restricted by water depth, and  $C/U_{*a}$  depends on depth and decreases linearly with wind speed, thus increasing wind separation and white-capping. Equation 23 not only improved the fit for  $z_o$  but also improved the correlations between dimensionless wave parameters which use the resulting  $C_d$  values, as will be described later.

A depth-dependent function was needed to describe  $C_d$ . By substitution of a depth-limited wave model for  $H_s$ , presented later, and expressions relating  $C/U_{*a}$  to  $U_a$  and  $h$  into Equations 2, the following expression was found by trial and is proposed for shallow water:

$$C_d = \left( \frac{0.4}{16.11 - 0.5 \ln(h) - 2.48 \ln(U_a)} \right)^2, \quad h < 2 \text{ m} \quad (24)$$

Equation 24 predicts smaller  $C_d$  values than Equation 5 when  $h < \exp(3.25 - 1.2 \ln(U_a))$ , for example, when  $h < 1.6$  m at  $U_a = 10$  m/sec.

Estimated  $C_d$  values from Equation 24 are shown in Figure 13 along with values determined by use of Equation 23 for vegetated and bare stations in Laguna Madre. However, more comparisons to data are needed to determine the generality of Equation 24. It is difficult to discern the relative importance of depth and seagrass to  $C_d$  with available data, but it appears depth, or effective depth as discussed later, is more critical to  $C_d$  than seagrass is.

Fetch length is also a factor that affects  $C_d$  in enclosed waters and has been included in formulations presented by Hsu (1988). As indicated earlier, wave data from Laguna Madre indicate that previous fetch relationships developed from bare, slightly deeper, areas

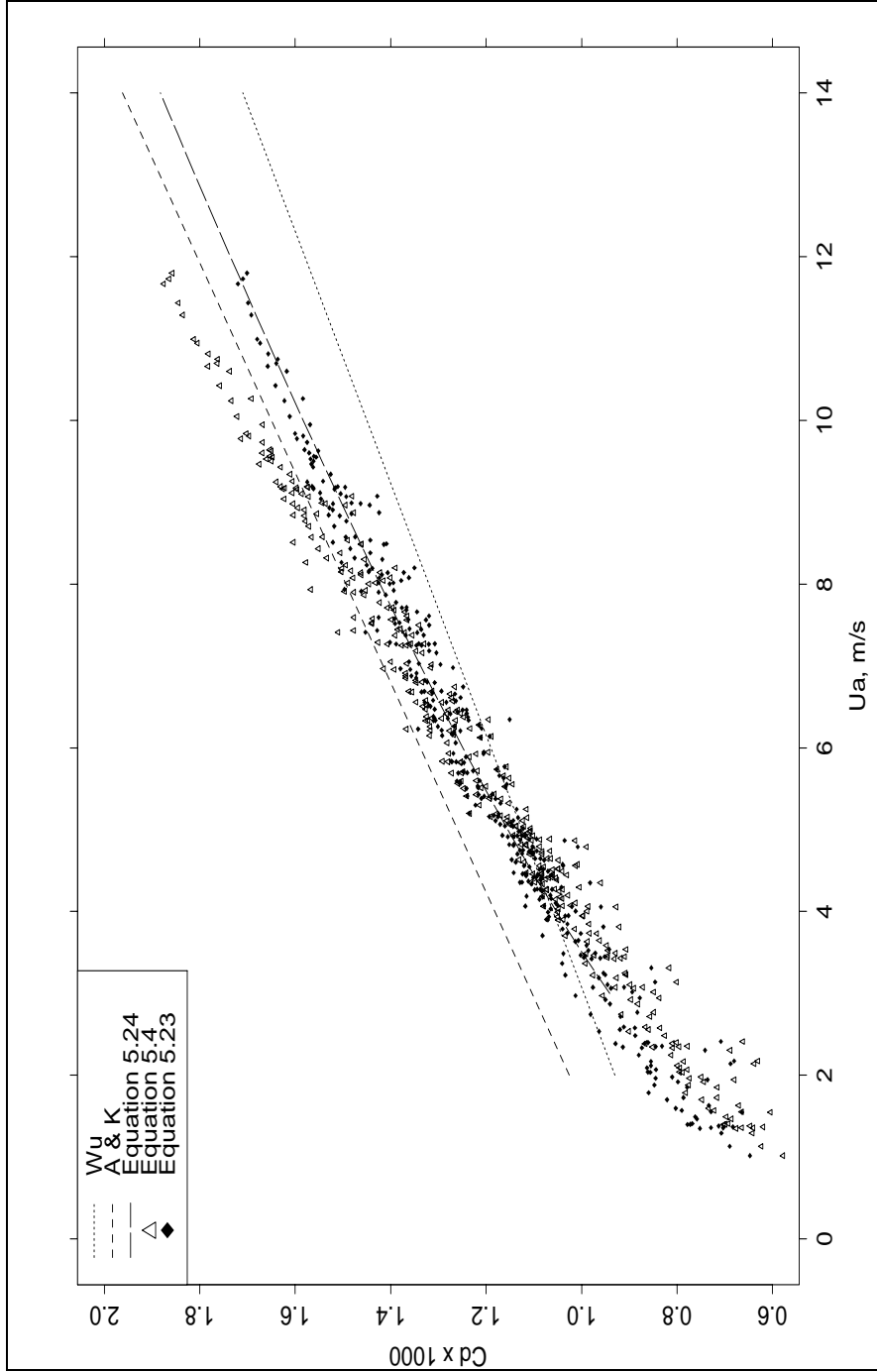


Figure 12. Comparison of atmospheric friction factors calculated based on Wu (Wu 1980), A & K (Atakturk and Katsaros, 1999), and Equations 4, 23, and 24

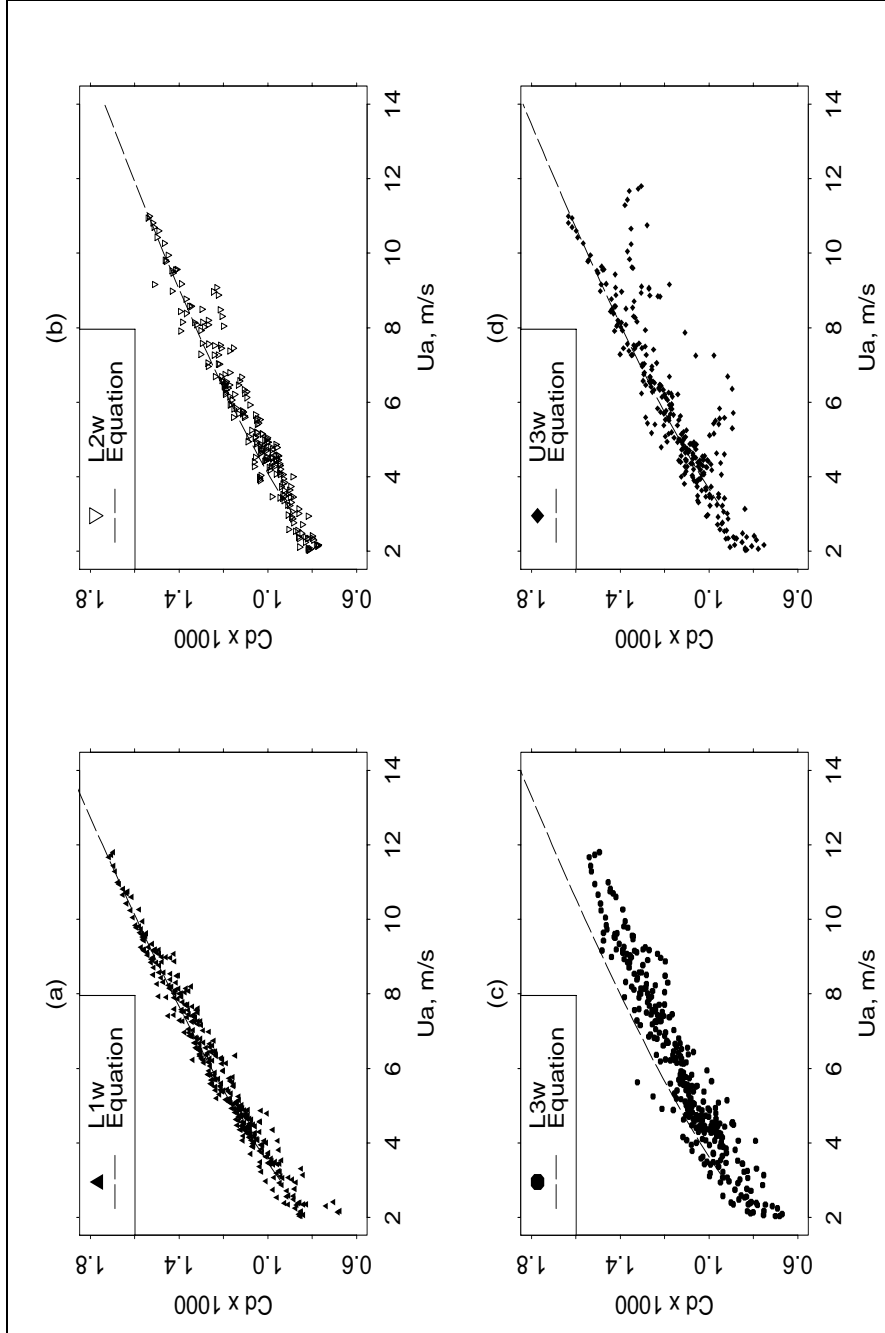


Figure 13. Comparisons of atmospheric friction factors calculated Equations 23 (symbols) and 24 (lines) for four measurement stations

should be used with caution. The difference here may be that, for seagrass areas with high wave-frictional dissipation, the ratio of wave energy to energy dissipation is smaller than for bare, deeper areas. Where momentum is transferred from the atmosphere to small wave lengths, waves build more quickly to a steady condition in which input and dissipation of momentum balance.

### Shear stress budget

Charnock's parameter decreases with wind speed, so that according to Equation 9, almost all shear stress is transferred to waves at low wind speeds, and greater portions of  $\tau_a$  are dissipated by white-capping and/or water-column mixing, and less of the total input is dissipated by wave friction at higher wind speeds. Wave dissipation as a result of mixing was not considered, since the lagoon system is normally wind-mixed and tends to be vertically homogeneous. Wave breaking by excess steepness or relative depth was not observed in the Laguna Madre.

For fully-developed waves (constant wave spectra), wave dissipation through total friction and white capping is assumed to be equal to the atmospheric shear stress at the water surface. Even when only a few percent of  $\tau_a$  goes directly into currents as  $\tau_{ac}$ , some part of  $\tau_{aw}$  is subsequently transferred to  $\tau_{ac}$  by white-capping, thus,  $\tau_a$  is assumed to be partitioned between shear stress imparted to waves ( $\tau_{aw}$ ) and to currents ( $\tau_{ac}$ ):

$$\tau_a = \tau_{aw} + \tau_{ac} \quad (25)$$

Ratios of  $\tau_{aw}/\tau_a$  were computed (after the unknown roughness height  $k_n$  was removed) with Equations 1 to 2, 12, 14 to 16, and 23. The peak wave shear stress is 2.38 times the average shear stress. Regressing this ratio against wind speed gives an indication of the amount of atmospheric shear stress going into wave shear stress. By assuming that almost all atmospheric shear stress goes into waves at wind speeds 3 to 5 m/sec where a peak in the ratio occurred (assumed to be 0.97), results indicated that the amount decreases at higher wind speeds as

$$\frac{\tau_{aw}}{\tau_a} = 2.169 U_a^{-0.5}, \quad U_a > 5 \text{ m/sec} \quad (26)$$

Plots of  $\tau_{aw}/\tau_a$  calculated by Equations 26 and 9 versus wind speed are shown in Figure 14 for L1w. Charnock's parameter was calculated with Equations 6 and 23 and was higher than reported values for open waters. Since  $\alpha_c$  did not approach the previously cited value of 0.012 for "old" waves, the fraction of shear stress going into waves remained high. Computed values of  $\tau_{aw}/\tau_a$ , which lead to Equation 26, had a great deal of scatter, as can be seen in Figure 14. The regressions for L1w had  $M-R^2 = 0.09$ ,  $p\text{-value} < 0.01$ , and the resulting exponent = -0.435. The regression for L2w had  $M-R^2 = 0.15$ ,  $p\text{-value} < 0.01$ , and the resulting exponent -0.66. Equation 26 is, therefore, only approximate. Another possible way to determine  $\tau_{aw}/\tau_a$  is to determine  $1 - \tau_{ac}/\tau_a$  instead. This calculation might be done by determining water surface slope and velocity along the direction of the wind, and therefore the atmospheric shear stress going into the currents. Depth information indicated that at times of  $U_a < 5$  m/sec, the water surface slope between L1w and L2w did not vary. At higher wind speeds variation in water levels of 0.1 m occurred. Experience in applying

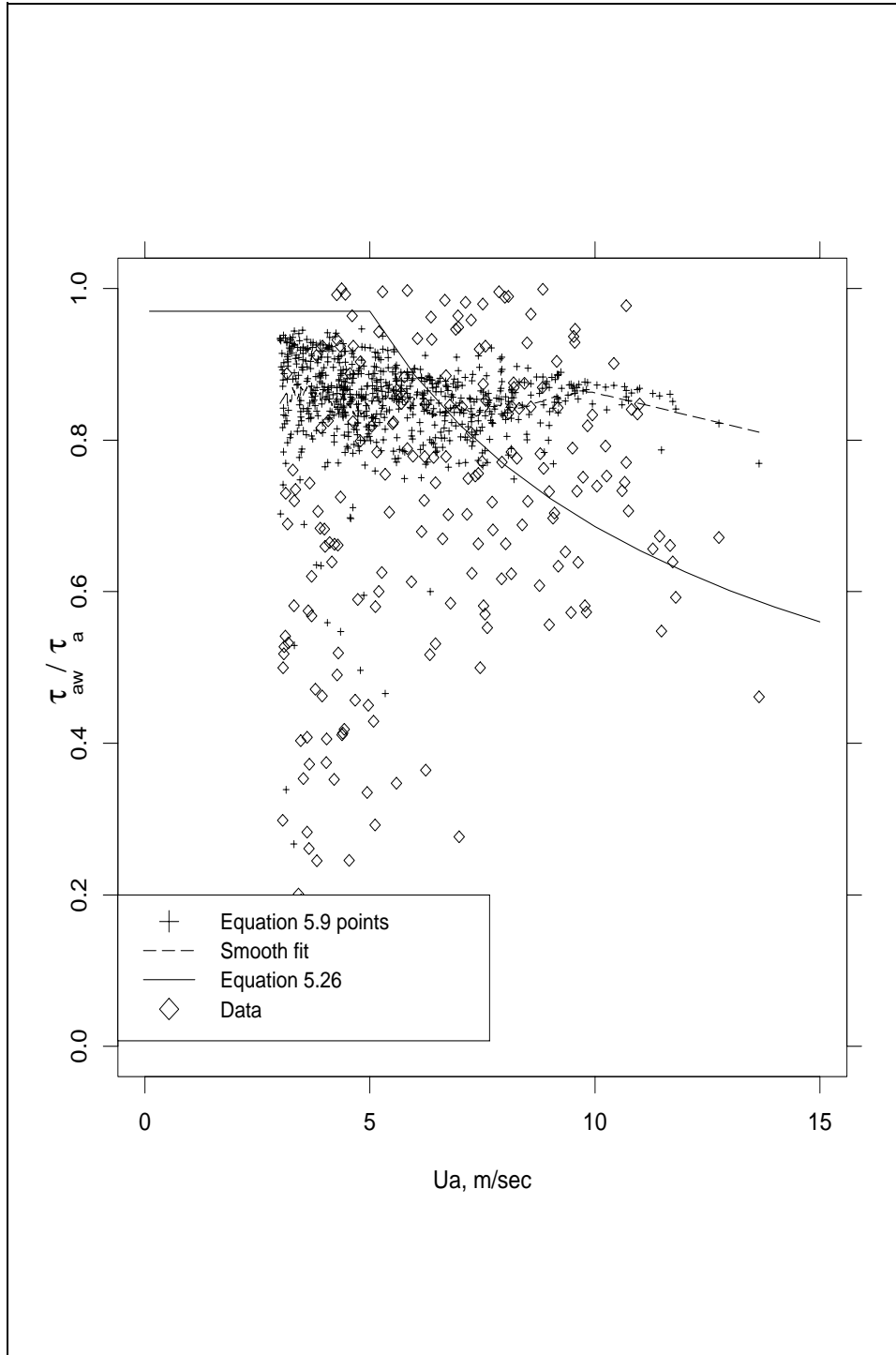


Figure 14. Ratios  $\tau_{aw}/\tau_a$  calculated according to Charnock's parameter and Equation 9, Equation 26, and wave characteristics and atmospheric shear stresses

hydrodynamic models to other systems has indicated that an appreciable fraction of shear stress must go into currents in order to reproduce observed water-level fluctuations. Equation 26 should be used with caution.

### **Depth-limited waves with high bed roughness effects**

Wave data from the station U1w, located in southern Corpus Christi Bay, was found to be different from data for those gauges located within Laguna Madre. That station was slightly deeper than those in Laguna Madre proper and provided a valuable contrast of a different shallow-water wave climate. Dimensionless wave energy  $E^*$  values are plotted against  $h^*$  in Figure 15a for station U1w for all wind and for the optimal wind conditions described earlier. The values for the uniform wind condition identified earlier were suspected of being optimum for comparisons and were separated out from the remainder of the data. The data centered at  $130^\circ$  wind direction were largely a super-set of the uniform wind set and were not used separately. Also plotted in Figure 15a are CERC (1984) and Young and Verhagen (1996) fits to Equation 10, which should correspond to the upper edge of the scattered data. Fetch limitations bring values downward away from this line. It appears that the CERC (1984) coefficients make Equation 10 more parallel to the upper edge, although if some data errors were admitted, a slight reduction in  $a$ , might be warranted. Scatter of the data in Figure 15a is similar to the data presented by Young and Verhagen (1996).

Dimensionless wave energy  $E^*$  values are plotted against  $h^*$  in Figure 16 for all other stations except U2w. The data set from station U2w had only 219 points total and 71 points in the uniform-wind set, only about one-third as many points as the next smallest data set, and, therefore, will be omitted from subsequent data analyses. The  $E^*$  versus  $h^*$  data scatter can be seen in Figure 16 as more tightly banded than for U1w, especially as individual stations, but the edge of the scattered data is displaced downward from previous equation fits. Station L2w is located in dense *Thalassia* seagrass, and these plotted  $h^*$  values were computed with  $h$  adjusted -0.2 m to allow for the seagrass canopy. *Thalassia* sp. was the most resistive to currents of those tested by Fonseca and Fisher (1986).

Dimensionless frequency  $f^*$  values are plotted against  $h^*$  in Figure 15b for U1w. The depth-limited case falls on the lower edge of the data scatter and can be compared to the previous results from CERC (1984) and Young and Verhagen (1996) in this plot. The slope implied by the present data scatter is different from these previous studies. Results for L1w, L2w, L3w, and U3w are shown in Figure 17. As with  $E^*$  versus  $h^*$ , the collective- and individual-station scatter away from the depth-limited case, as described by Equation 11, is less for these stations than for U1w and previous studies.

The effect of fetch length on wave conditions can best be examined with use of data from L1w and L2w, which were located inline with each other in the dominant wind direction ( $110^\circ$  to  $145^\circ$  with a mean of  $128^\circ$ ) and had more uniform depth along this direction. Fetch lengths differed by a factor of two for this wind direction, 10.2 and 5.1 km respectively. Following Young and Verhagen (1996),  $E^*$  versus  $\chi^*$  for increments of small  $h^*$  (high winds) were plotted in accordance with data from L1w and L2w as shown in Figure 18. Bounding curves for  $h^*$  values were plotted as described by Equations 12 and 13. Based on

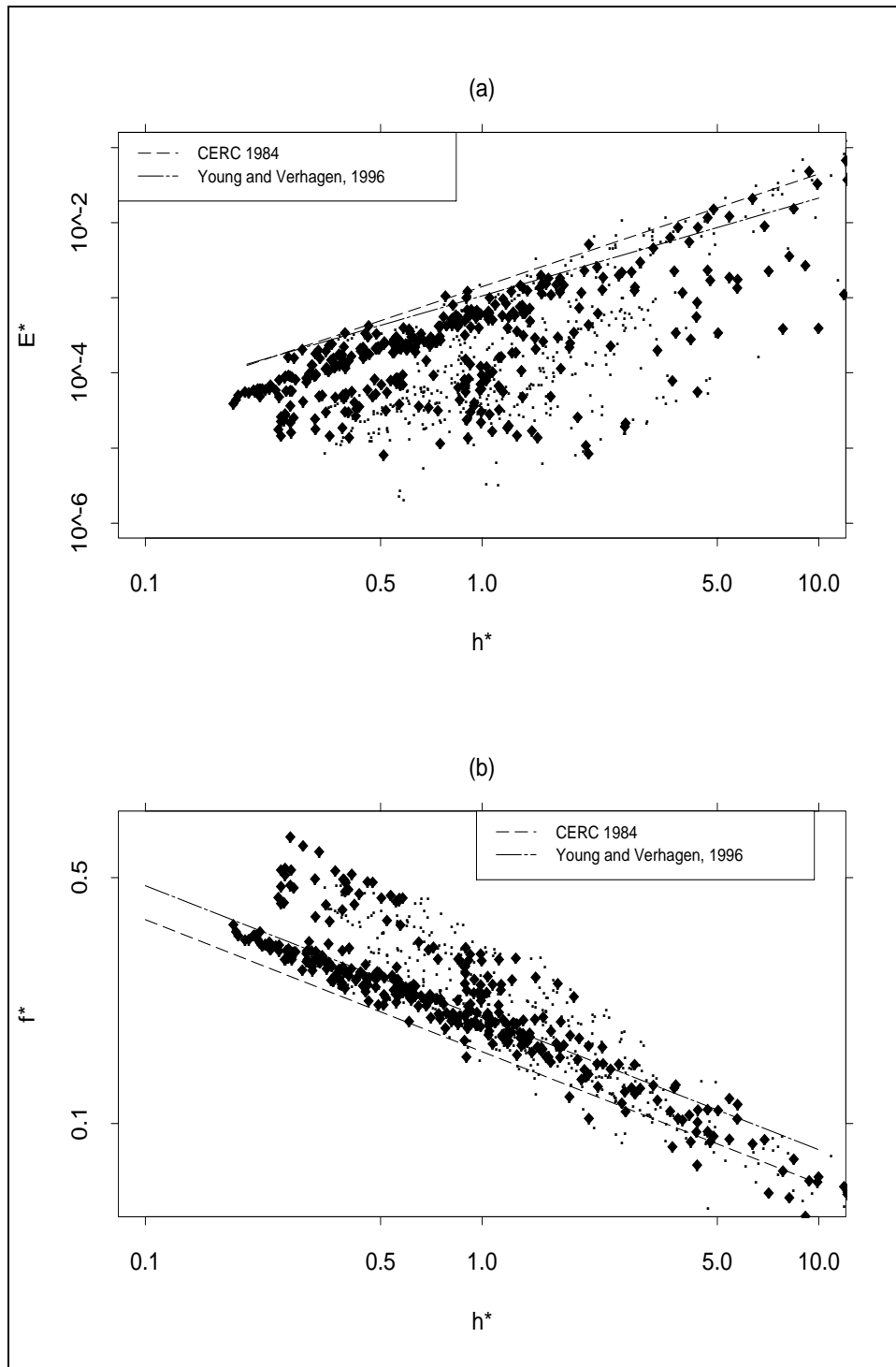


Figure 15. Dimensionless wave parameters for station U1w (diamonds are optimum winds and dots are all other winds) with model fits: (a) wave energy versus depth, and (b) wave frequency versus depth

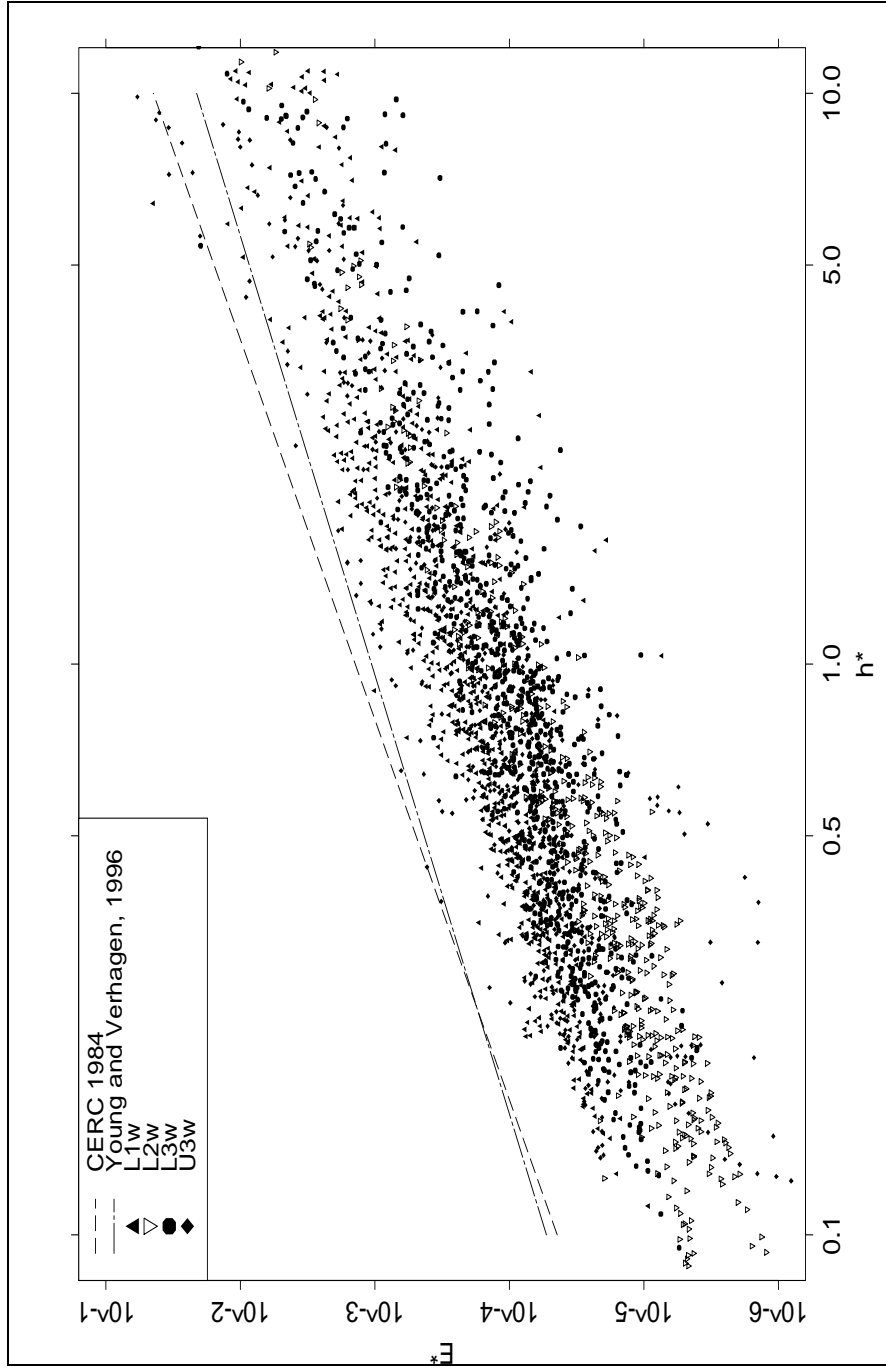


Figure 16. Dimensionless wave energy  $E^*$  versus depth  $h^*$  for four Laguna Madre measurement stations with model fits

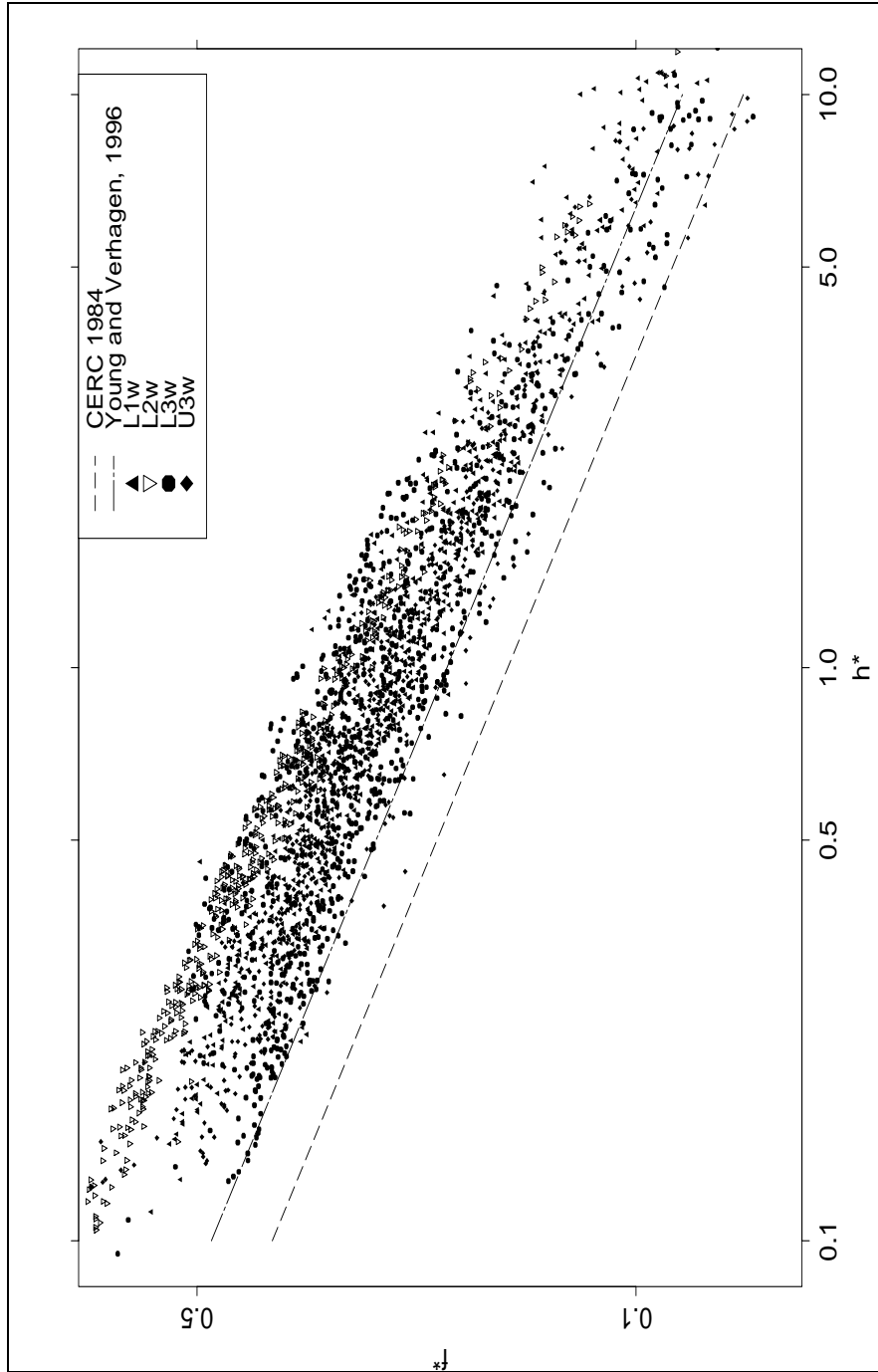


Figure 17. Dimensionless wave frequency  $f^*$  versus depth  $h^*$  for four Laguna Madre measurement stations with model fits

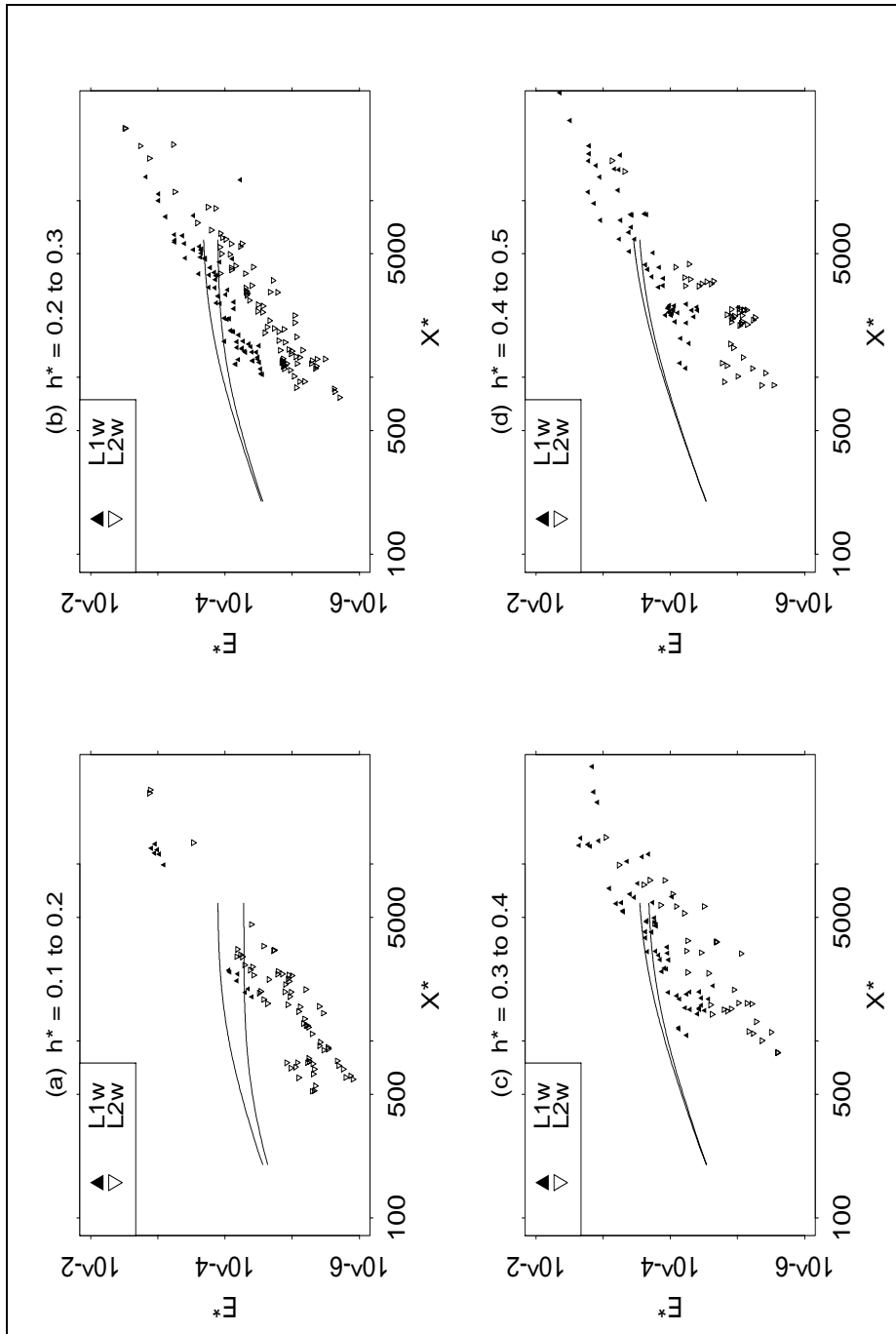


Figure 18. Dimensionless wave energy versus fetch length  $\chi^*$  at stations L1w and L2w for four ranges of  $h^*$

those equations, data should plot between the curves presented. Data from Laguna Madre diverge sharply from the results of previous studies with regards to the effect of fetch length, as can be seen from Figure 18. The data scatter suggests a constant slope of about two. However, since  $E^*$  is a function of  $U_a^{-4}$  and  $\chi^*$  is a function of  $U_a^{-2}$ , a slope of 2 represents a spurious correlation between these two parameters (Young and Verhagen 1996). Such a relationship would suggest that wave height is related only to fetch length (that is a constant for this wind direction) and not related to wind speed. It appears that the customary values of dimensionless fetch  $\chi^*$  do not describe the effect of fetch in the Laguna Madre data.

Apparently, fetch effects occur over much smaller  $\chi^*$  in Laguna Madre than previously found, possibly due to high bottom frictional effects. The lack of fetch effects is also reflected in the relatively low data scatter about the trends shown in Figure 16. Since in this case the depth-limited wave condition is not an asymptote but is assumed to be the main tendency of the data, fits to the data were made through this central tendency rather than at the edges of the scattered data. Scatter about this tendency is considered to be introduced by various errors and not importantly by the effects of fetch.

More appropriate scaling for dimensionless wave energy and wave frequency in ultra-shallow water was found by use of the atmospheric friction velocity,  $U_{*a} = C_d^{0.5} U_a$ , in place of  $U_a$ . The wave-model expressions corresponding to Equations 10 and 11 are

$$E^{\cdot} = a_5 h^{*a_6} \quad (27)$$

$$f^{\cdot} = a_7 h^{*a_8} \quad (28)$$

where the new dimensionless parameters  $E^{\cdot}$  and  $f^{\cdot}$  equal  $g^2 E / (C_d^2 U_a^4)$  and  $C_d^{1/2} U_d / (g T_p)$ , respectively. With these scalings, data were brought closer into line (with higher M-R<sup>2</sup> value) when plotted against  $h^*$ , as shown in Figures 19 and 20, than in the comparisons shown in Figures 16 and 17. Regressions were performed between  $E^{\cdot}$  and  $h^*$  with data subsets for uniform wind, winds greater than 3 m/sec, and  $H_s$  values greater than the 25<sup>th</sup> percentile conditions. Results yielded exponents  $a_6$  for  $h^*$  of between 1.73 and 2.11. The assumption of an exponent of 2.0 implies that  $H_s \propto C_d h$ , and regression with this form yielded the following empirical expression:

$$H_s = 84.6 h C_d - 0.056 \quad (29)$$

(M-R<sup>2</sup> = 0.765, RSE = 0.0253 m, n = 2056) where the intercept is apparently caused by the range of  $C_d$  which does not converge to zero at zero wind speed. Plots of observed versus calculated  $H_s$  for the four stations are shown in Figure 21.

Regressions performed between  $f^{\cdot}$  and  $h^*$  indicated an exponent  $a_8$  of -0.5, thus  $T_p \propto (h C_d / g)^{1/2}$  and further analysis indicated that

$$T_p = 126.5 (h C_d / g)^{0.5} \quad (30)$$

(M-R<sup>2</sup> = 0.982, RSE = 0.241 sec, n = 2056). Plots of observed versus calculated  $T_p$  for the four stations are shown in Figure 22.

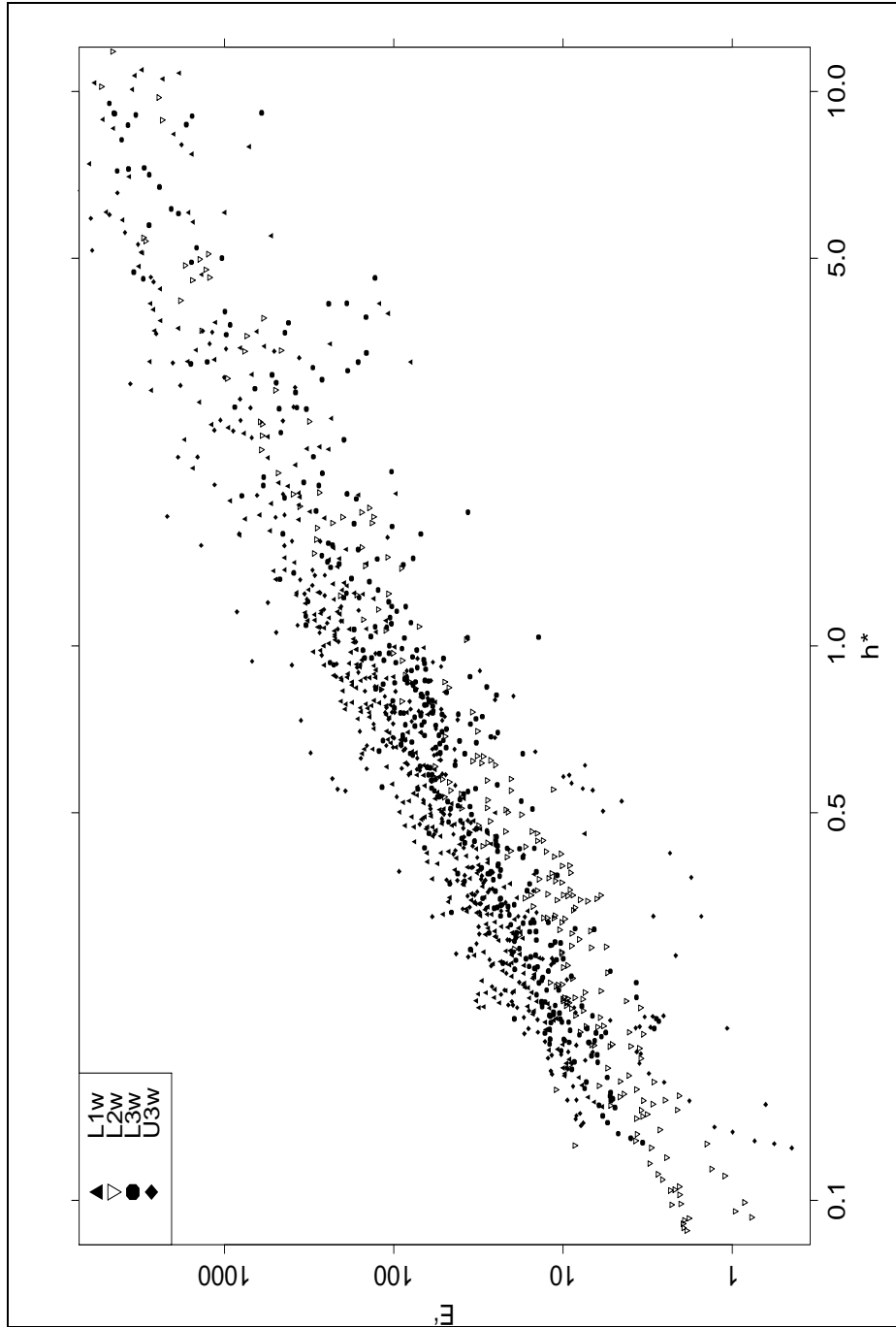


Figure 19. Dimensionless wave energy  $E'$  versus depth  $h^*$  for four Laguna Madre measurement stations

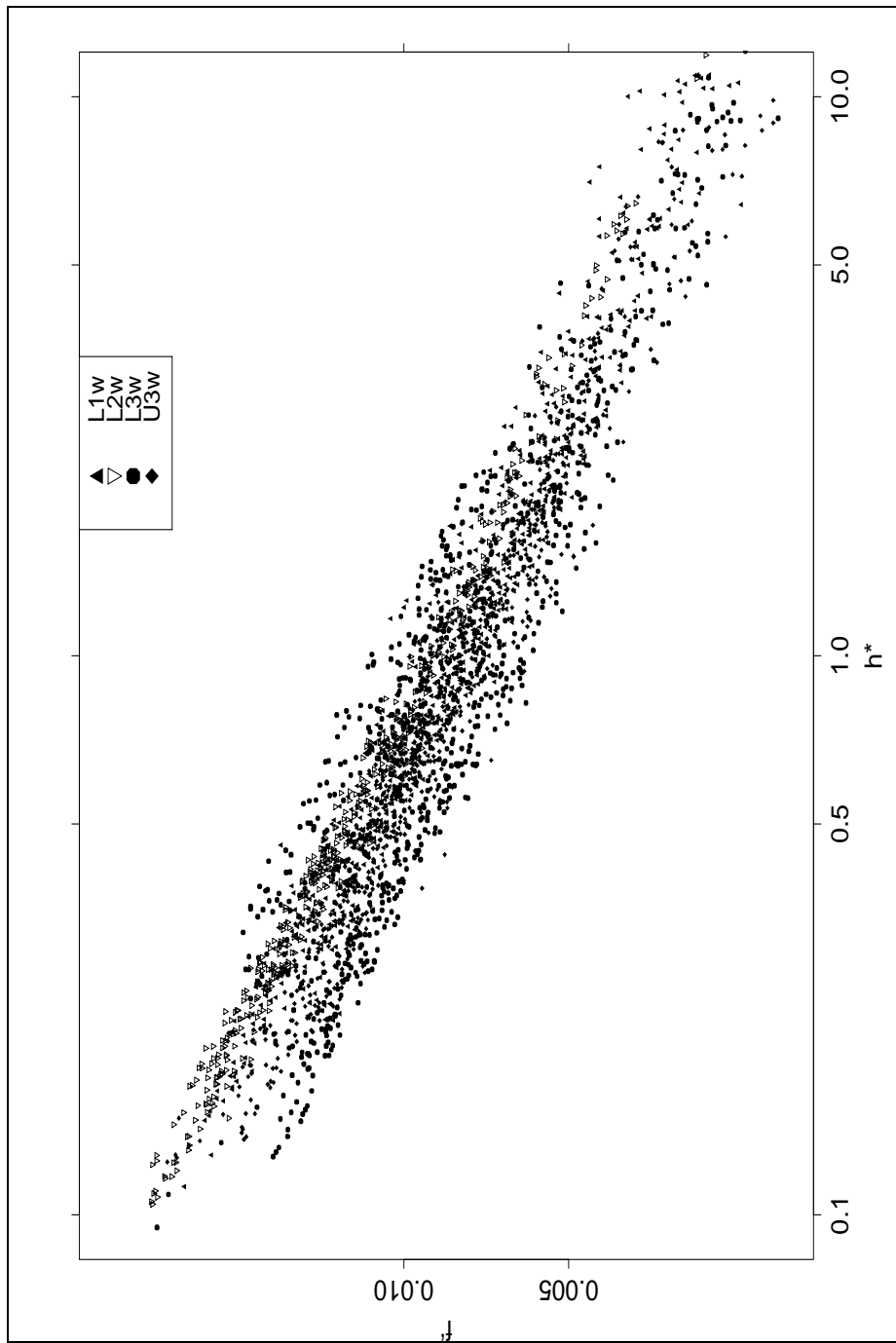


Figure 20. Dimensionless wave frequency  $f^*$  versus depth  $h^*$  for four Laguna Madre measurement stations

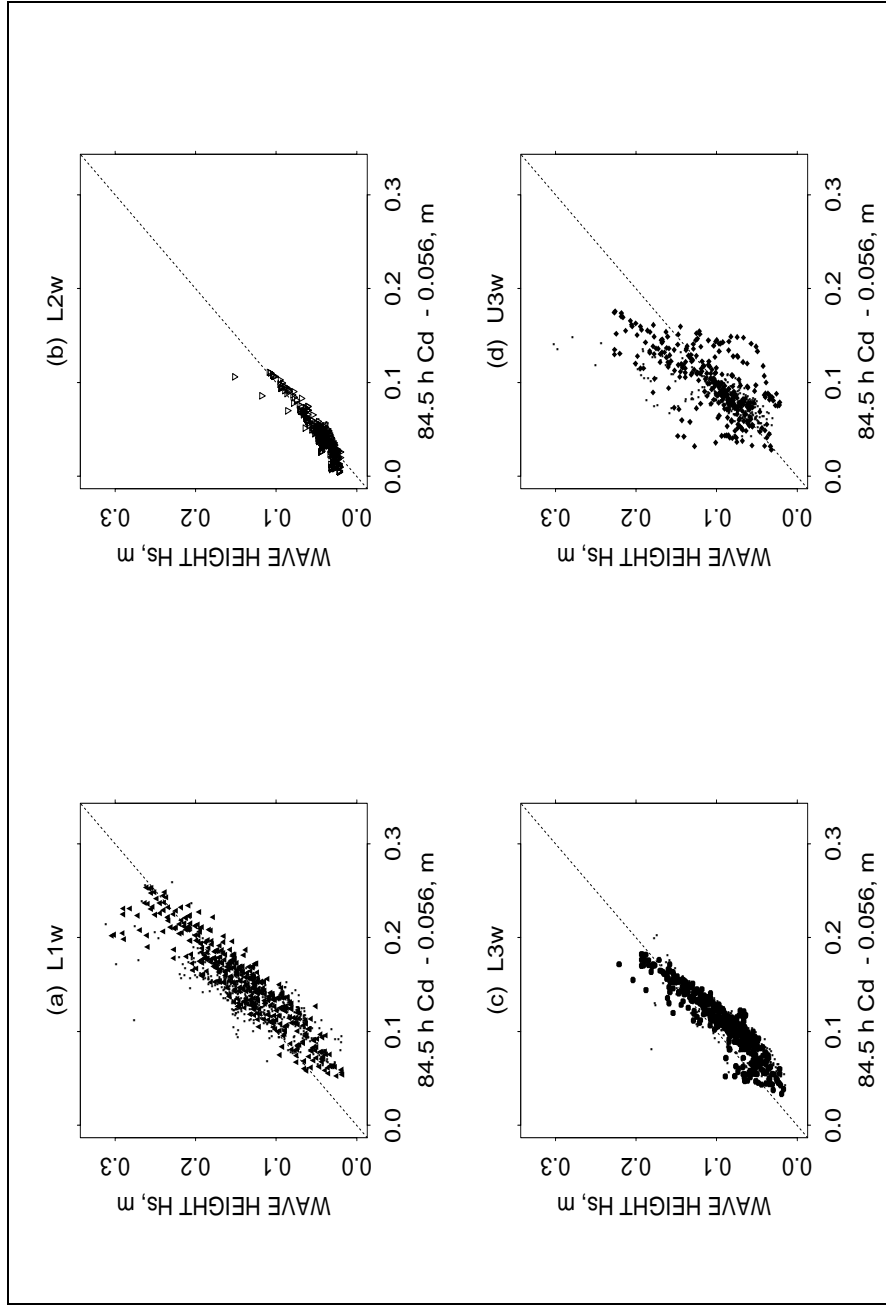


Figure 21. Significant wave heights computed with Equation 29 versus observed values for four Laguna Madre stations

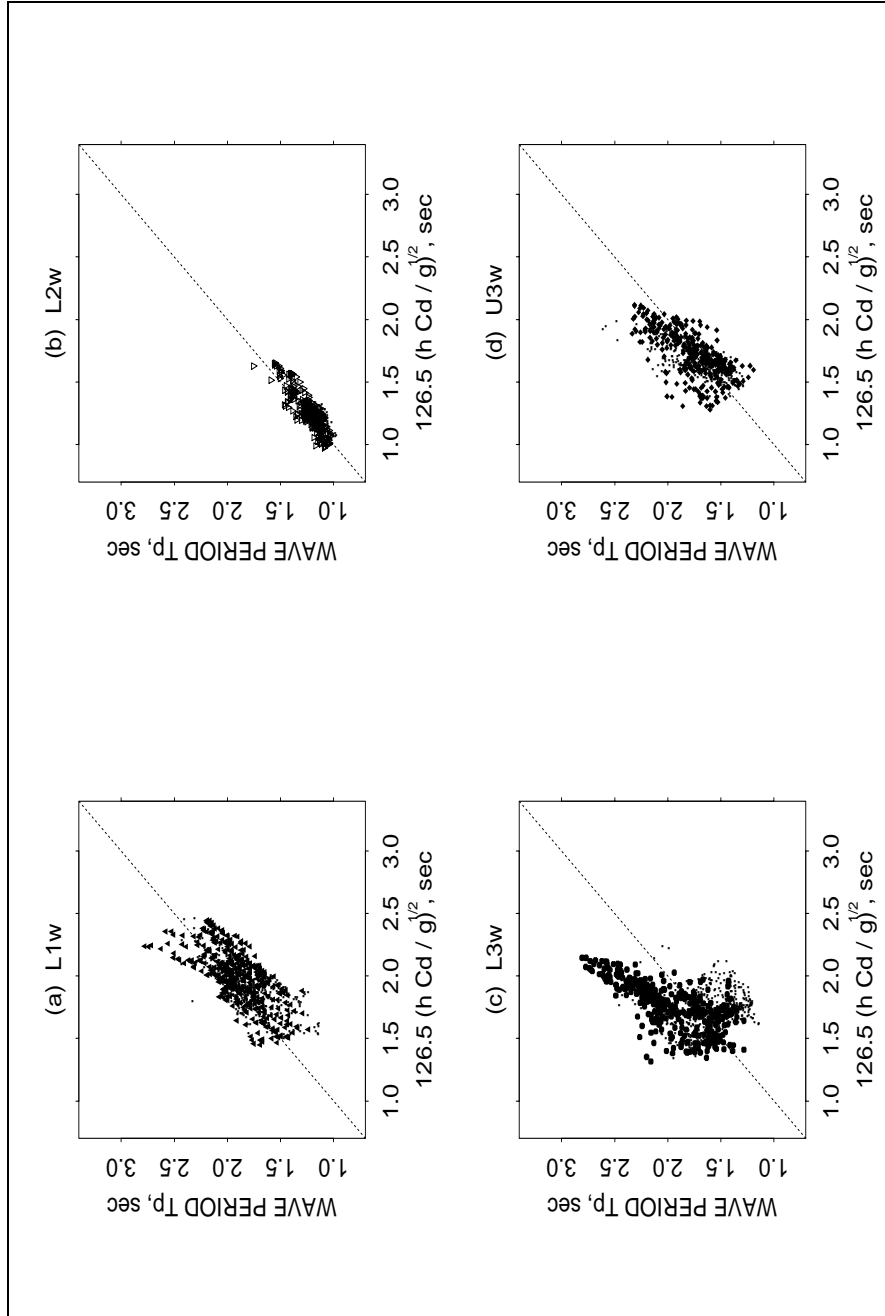


Figure 22. Peak wave periods computed with Equation 30 versus observed values for four Laguna Madre stations

## Wave friction factors

Wave shear stresses  $\tau_w$  were estimated with laminar, turbulent, and transitional laminar/turbulent frictional formulations. Computation of laminar shear stresses was based on observed wave characteristics and Equations 14-17, and results were correlated to computed  $\tau_a$  values. The laminar friction formulation produced shear stresses which were often higher than the atmospheric shear stress input. Even though the laminar formulation is often used for shallow-water resuspension calculations, it appears to be physically unrealistic in this case. Currents at these sites are low but almost always above threshold values required to produce turbulent water-column conditions. Apparently a wave-current interaction occurs through the eddy-viscosity profile whereby waves assume the turbulent condition of the water column even at low wave Reynolds numbers.

The turbulent rough formulation (Equation 18) had consistently higher correlations than the other formulations for the six stations. A wave model was developed which used iteration to arrive at a fully-developed wave height and period, matching observed values reasonably well, and in balance with atmospheric shear stress and dissipation. Turbulent-rough-bottom friction described by Equation 18, and wave breaking dissipation calculated according to the method of Massel and Belberova (1990) were included in the model formulation. Whitecapping and dissipation from spectral wave interactions were lumped together as one dissipation mechanism, and shear stress partitioned according to Equation 9.

The wave model was validated by a comparison of observed and model wave height distributions and by a comparison of computed shear stresses to observed wind shear stresses. The main results were the estimates for the roughness height,  $k_n$ , at the Lower Laguna Madre stations, which are presented in Table 7.

Station	$k_n$ , m	Median peak $\tau_w$ , Pa	Median $\tau_a \times 2.38$ , Pa	Median $H_s$ , m
L1w	0.0014	0.049	0.058	0.133
L2w	0.2	0.044	0.065	0.044
L3w	0.01	0.053	0.051	0.083

The atmospheric shear stress, factored by 2.38, was added to Table 7 for comparison to the peak-wave shear stress. The estimated roughness heights are consistent with the bottom type, where L1w is bare bottom, L2w is thick seagrass bed, and L3w is seagrass edge. The peak shear stresses were predicted to be not much different for these stations even though wave heights were very different.